Nanoscale

REVIEW

View Article Online
View Journal | View Issue

Cite this: *Nanoscale*, 2025, **17**, 15110

Advancing extracellular vesicle production: improving physiological relevance and yield with 3D cell culture

Kara Cook and Huiyan Li *

Extracellular vesicles (EVs) are essential nanoscale mediators of intercellular communication, holding significant potential as early disease biomarkers and therapeutic agents. Present in biological fluids like blood, EVs and their molecular cargo can be detected in liquid biopsies for diverse diagnostic and therapeutic applications. However, the availability of patient samples is often limited for such research. To tackle this challenge and gain insights into *in vivo* disease mechanisms, *in vitro* production of EVs from the cell culture models that closely mimic *in vivo* conditions has become an essential tool. While 2D cell culture has been the standard for high-throughput studies for decades, 3D cell culture is emerging as a more physiologically relevant *in vitro* tool for mimicking *in vivo* environments and providing deeper insights into disease. However, there is currently a lack of literature synthesizing and comparing the effects of 3D *versus* 2D cell culture models on EV production and analysis. In this review, we examine recent studies that compare the impacts of 3D and 2D cell culture models on EV yield, composition, and functionality. We categorize 3D models into subtypes, including spheroids, hydrogels, rigid scaffolds, and bioreactors. Details of each model's impact on EVs compared to 2D cell culture are presented. Furthermore, we discuss the advantages and limitations of these 3D models as identified in individual studies, offering insights to guide future research directions in this evolving field.

Received 17th February 2025,
Accepted 10th June 2025

DOI: 10.1039/d5nr00707k

rsc.li/nanoscale

1. Introduction

Extracellular vesicles (EVs) first gained significant attention in the early 1980s when platelets were discovered to release small

School of Engineering, University of Guelph, Guelph, Ontario, Canada N1G2W1. E-mail: huiyanli@uoguelph.ca; Tel: +1 519 824 4120 ext. 54699

Kara Cook

Kara Cook completed her B.Sc. in Biomedical Science at the University of Guelph, Canada and is currently pursuing a Master of Applied Science in Biomedical Engineering at the same institution. Her research focuses on the production and characterization of cancer extracellular vesicles (EVs) using 2D and 3D cell culture platforms. She aims to identify novel EV-based biomarkers for the early detection of cancer, contributing to improved diagnostic strategies and patient outcomes.

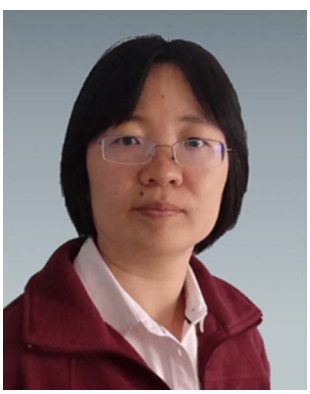

Huiyan Li

Huiyan Li received her PhD in Biomedical Engineering at McGill University, Canada. After a postdoc training in UVic-Genome BC Proteomics Center, Dr Li joined the Biomedical Engineering group as a research fellow at Harvard Medical School – Massachusetts General Hospital. In 2020, Dr Li joined the University of Guelph and started her research lab. Her research focuses on developing micro- and nano-technologies for the study of health and diseases, with a particular interest in developing novel technologies for analyzing extracellular vesicles (EVs). Her work has been published in top peer-reviewed journals and has been highlighted in major scientific magazines.

membrane-bound vesicles.[1–3] Since then, research has revealed their critical role in intercellular communication and biological processes, such as cancer progression, positioning them as promising disease biomarkers and therapeutic agents.[4–11] EVs are nanoscale particles released by cells into the surrounding extracellular environment, carrying biomolecular cargo such as nucleic acids, proteins, and lipids from their parent cells.[5,6,12] They influence neighboring cells through cargo delivery and expression of surface markers that facilitate cell targeting and activate intracellular signaling pathways.[12–14] Additionally, EVs function in waste management by removing damaged metabolic components.[15] EVs are divided into three primary types: exosomes, microvesicles, and apoptotic bodies, distinguished by their composition, size, biogenesis, and function.[16] Secreted by organisms ranging from prokaryotes to mammals, EVs can be isolated from all bodily fluids, such as blood, saliva, and urine, making them easy to detect in liquid biopsies.[12]

EVs are gaining attention as effective biomarkers for disease diagnosis and prognosis due to their overexpression in various diseases, their role in intercellular communication, and their ability to preserve the molecular cargo of their parent cells.[17] Studies are increasingly exploring the use of EVs and their cargo for early disease detection.[18–27] While many of these studies have focused on analyzing patient-derived EVs from bodily fluids such as urine and plasma, patient samples are scarce, limiting their availability for high-throughput biomarker screening.[18,19,21,22,27] To address this, *in vitro* models, particularly cell culture, are essential for investigating the molecular characteristics of EVs and enabling high-throughput analyses. Cell culture allows researchers to grow and maintain cells outside their natural environment, providing a controlled system to study disease characteristics and drug responses.[28] This method has played a crucial role in EV biomarker discovery, particularly for diseases like breast and prostate cancer, through the culture of disease-specific cell lines, media collection, EV isolation, and subsequent analysis.[29,30]

Since the early 1900s, 2D cell culture has been the gold standard for cell biology research, disease-modeling, and drug discovery, leading to breakthroughs such as studying the effects of antibiotics on tissues,[31] developing polio vaccines,[32] creating specialized cell lines,[33] and reprograming adult cells into induced pluripotent stem cells (iPSCs).[34] However, 2D culture oversimplifies key *in vivo* features, including the microenvironment, intercellular communication, and cell morphology.[35] In response, various 3D culture techniques are increasingly being used to better replicate *in vivo* conditions by supporting the growth of cells within three-dimensional matrices.[36]

Currently, a wide range of 3D cell culture models are available, broadly categorized into scaffold-free and scaffold-based methods.[37] Scaffold-free models, like spheroids, rely on cell-to-cell adhesion to self-assemble into 3D aggregates in suspension, often utilizing platforms like ultra-low attachment (ULA) plates.[37,38] Whereas, scaffold-based method, including hydrogels, rigid scaffolds, bioreactors, and microcarriers, use exogenous materials to mimic the native extracellular matrix, providing structural integrity.[37]

Recent studies have compared the effects of novel 3D cell culture with conventional 2D culture on EV productions, focusing on aspects such as EV secretion, morphology, cargo content, and functionality. This emerging body of research highlights the significant differences in vesicle production and composition between the two culture systems, suggesting that 3D models may better mimic the *in vivo* environment and influence cellular behavior more effectively, as demonstrated through higher EV yields with increased activity, complexity, and similarity to native EVs.

This review aims to comprehensively evaluate the impact of 3D *versus* 2D cell culture models on EV production, cargo, and function. While previous literature has investigated the impact of cell culture conditions, such as cell passage and EV isolation techniques, on some aspects of EV properties and functionality, existing reviews focus on specific model types and lack direct comparisons between 2D and different 3D systems.[39,40] This review is, to our best knowledge, the first to investigate the impact of various 3D *versus* 2D culture models on EVs by synthesizing findings from multiple primary studies. By comparing these models across studies, we identify their relative advantages, limitations, and translational potential for EV-based diagnostics and therapeutics, providing a roadmap for future innovation in EV research.

2. Comparing the characteristics of EVs collected from 2D *vs.* 3D cell culture

The following section is organized by 3D cell culture models (Fig. 1 green box), beginning with scaffold-free spheroids, followed by scaffold-based approaches, which are further categorized into hydrogels, rigid scaffolds, and bioreactor systems.

2.1 Scaffold-free 3D models: spheroids

2.1.1 Low attachment culture plates and dishes. Low attachment (also referred to as non-adherent) plates prevent cell attachment to the surface, promoting 3D spheroid formation through cell-to-cell aggregation.[41] These plates are often coated with a hydrophilic polymer, like poly-HEMA, that minimizes protein and cell adhesion.[42] Major advantages of low-attachment culture vessels include their low cost, ease of implementation, and ability to promote cell-to-cell adhesions, making them particularly useful for modeling *in vivo*-like conditions.[43] However, protocols often require centrifugation, which can introduce shear stress and lead to cell damage.[43] Larger spheroids may also experience limited oxygen and nutrient diffusion, leading to necrotic cores.[44] Additionally, these systems lack extracellular matrix (ECM) components that are found in scaffold-based models and do not provide the dynamic culture conditions offered by bioreactors, limiting

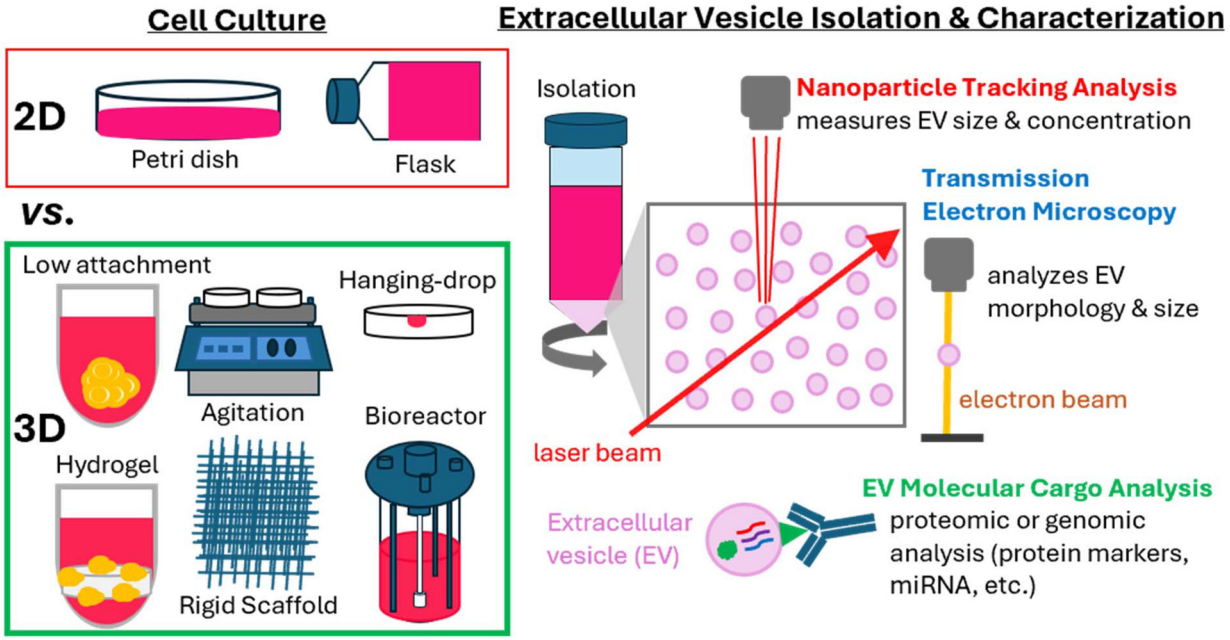

Fig. 1 Schematic illustration of the various 2D and 3D cell culture techniques and their downstream EV analyses.

their physiological relevance compared to more advanced 3D culture systems.[44]

2.1.1.1 Non-adherent microwell plates. One study compared EVs derived from PANC-1 pancreatic cancer cells cultured in 3D spheroids using ultra-low attachment (ULA) 96-well plates *versus* 2D monolayers in 24-well plates.[41,45] Spheroids were formed by centrifuging cell suspensions and incubating on a rotary shaker for 24 hours. After 24 hours, compact spheroids were retained, and loose aggregates were discarded. On Day 5, conditioned media (supplemented with 10% exosome-depleted fetal bovine serum (FBS)) were collected from both models, centrifuged to remove debris, and exosomes were isolated using a commercial kit and 220 nm filtration.

Transmission Electron Microscopy (TEM) showed EVs primarily ranged from 40–150 nm, though size distribution differences between 2D and 3D conditions were not assessed. Both TEM and RNA-selective stain fluorescence imaging revealed significantly higher EV secretion from 3D spheroids (Fig. 2A). Quantitative real-time PCR (qRT-PCR) analysis examined six specific miRNAs in 2D cells, 3D spheroids, and their corresponding exosomes (Fig. 2B). miRNA expression was consistently higher in exosomes than in parental cells. Among exosomal miRNAs, miR-96 showed no significant difference between 2D and 3D cultures, miR-4454 was significantly lower in 3D-derived exosomes, while miR-1246, miR-21, miR-17-5p, and miR-196a were significantly enriched in 3D-derived exosomes. Protein was extracted and quantified from exosomes and parent cells with a total exosome RNA & protein isolation kit, with GPC-1 levels measured *via* Enzyme-Linked Immunosorbent Assay (ELISA). Exosomes from 3D spheroids exhibited a 4-fold increase in GPC-1 levels compared to those from 2D cultures, as well as both 2D and 3D parent cells, suggesting that the 3D culture environment may enhance exosome sorting mechanisms ($P < 0.001$) (Fig. 2C).

Overall, this 3D scaffold-free culture generated spheroids that secreted significantly more EVs, enriched with specific genomic and proteomic cargo, offering valuable insights into disease mechanisms and pathways. Supporting the increased EV production in non-adherent 96-well plates, a study found that culturing bone marrow-derived mesenchymal stem cells (BM-MSCs) on poly-HEMA-coated 96-well plates led to a greater than 2-fold increase in EV production compared to 2D cultures by day 5 ($p < 0.001$).[42]

In contrast, a study comparing 2D and 3D cultures of BM-MSCs using non-adherent 96-well plates found no enhancement in EV yield, morphology, or cargo in the 3D model.[46] EVs were comparable across conditions, with 2D-derived EVs showing greater protein diversity. Interestingly, 3D-derived EVs exhibited pro-inflammatory and pro-fibrotic effects, indicating reduced therapeutic potential. The absence of EV enhancement may be due to the premature transition to serum-free media just 24 hours after cell seeding, which may have limited spheroid maturation.[47] Additionally, the high cell seeding density (2.5×10^4 cells per well) likely impaired nutrient and oxygen diffusion within the spheroids, reducing cell viability and EV secretion from the cells deep within the spheroid.[46]

2.1.1.2 ULA culture dish. While ULA microwell plates are commonly used for high-throughput 3D cell culture applications, ULA dishes provide a larger surface area that allows for the culture of more cells, offering distinct advantages in generating larger spheroids or aggregates in a more open

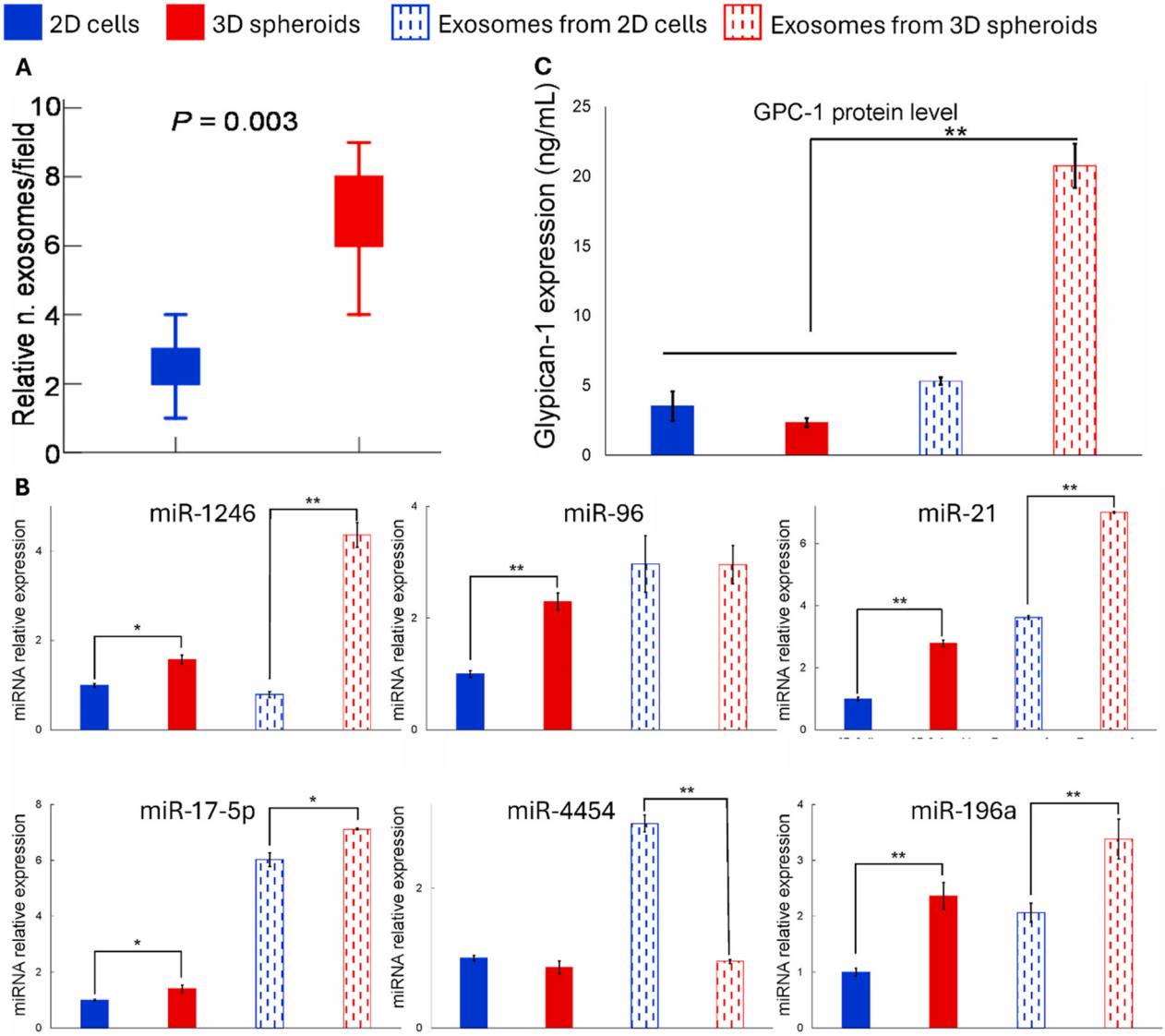

Fig. 2 Comparing exosome properties between 2D and 3D scaffold-free cell culture (A) quantity of exosomes per field (n = 5) observed from TEM analysis. (B) miRNA expression levels in 2D PANC-1 cells, 3D PANC-1 spheroids, and their exosomes, normalized to U6 and presented as mean ± SEM (*P < 0.05, **P < 0.01). (C) Glypican-1 (GPC-1) expression levels measured by ELISA in 2D PANC-1 cells, 3D PANC-1 spheroids, and corresponding exosomes. Results presented as mean ± SEM (**P < 0.01). Reproduced with permission from ref. 45. © 2021, Elsevier B.V.

culture environment. Exosomes from dental pulp stem cells (DPSCs) cultured as 3D spheroids in ULA dishes were compared to those from cells grown in monolayer flasks to assess their therapeutic efficacy on periodontitis and colitis.[48] Cells were grown in culture media with 10% exosome-depleted FBS. Exosomes were isolated from the cell media of both culture conditions using a multistep centrifugation process to remove debris, followed by ultracentrifugation and a PBS wash.

A Bicinchoninic Acid (BCA) Assay and Nanoparticle Tracking Analysis (NTA) revealed a significant increase in 3D-derived EV yields compared to 2D. NTA results showed that a 2-day culture of 1×10^7 DPSCs produced significantly more 3D-exosomes (3D-exos) per mL than 2D-exosomes (2D-exos) (Fig. 3A). Similarly, the BCA assay showed that 3D culture produced 2.23 mg of exosomes, significantly higher than the 0.36 mg yield from 2D culture (Fig. 3B). miRNA sequencing identified 28 differentially expressed miRNAs in 3D-derived exosomes compared to 2D, with miR-1246 showing the most significant change (8.58-fold increase). The 3D model revealed miR-1246s role in downregulating the Nfat5 gene, a regulator that inhibits Th17 differentiation. This downregulation helped restore the Th17/Treg balance, contributing to the amelioration of periodontitis and colitis.

The study also compared 3D-exos *vs.* 2D-exos' ability to suppress periodontitis and colitis using mouse models mimicking both diseases. Mice treated with 3D-exos had the greatest reduction in disease severity, demonstrated through the lowest alveolar bone loss (Fig. 3C), lower disease activity index scores (Fig. 3D), lower body weight loss (Fig. 2E), and longer colons

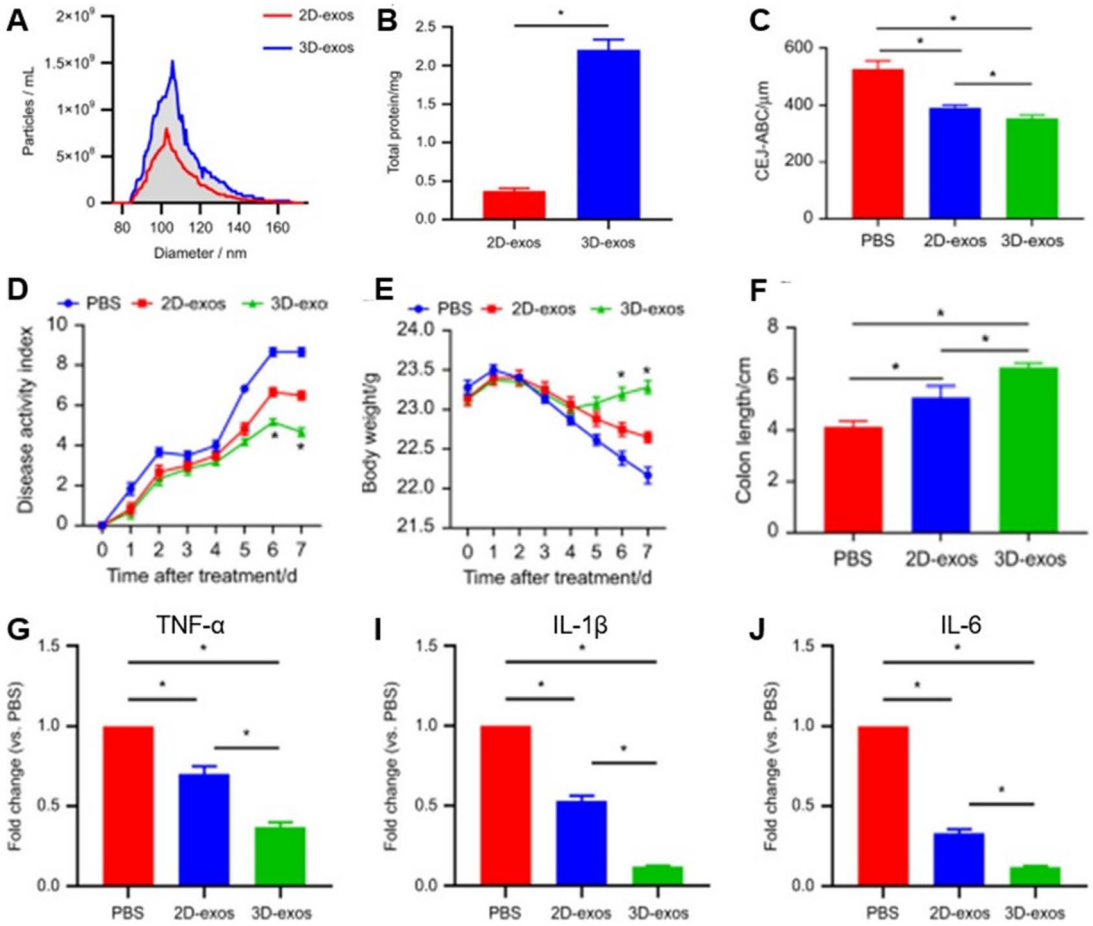

Fig. 3 EVs derived from DPSCs cultured in 2D (2D-exos) *versus* 3D spheroid cell culture (3D-exos). (A) NTA-generated particle sizes and concentrations of 2D-exos and 3D-exos. (B) 2D and 3D exosome yields quantified by BCA assays. (C) Alveolar bone loss in 2D-exos and 3D-exos evaluated by measuring the distance from the cementoenamel junction to the alveolar bone crest (CEJ-ABC). (D) Disease activity index (DAI) and (E) body weights in each group (n = 6). (F) Colon length in each group (n = 6 per group). (G–I) qRT-PCR analysis of TNF-α, IL-1β, and IL-6 gene expression levels in the colon across all groups (n = 6). SEM represented as error bars. *P < 0.05. Reproduced from ref. 48, under a Creative Commons Attribution 4.0 International License. © 2021, Springer Nature.

(Fig. 2F). 3D-exos also experienced reduced inflammation, showing fewer immune cells and lower inflammation in colonic tissues. Further, this can be corroborated with a RT-qPCR analysis which revealed 3D-exos reduced pro-inflammatory genes (IL-1β, IL-6, TNF-α) more effectively than PBS or 2D-exos (Fig. 2G–I).

The ULA culture of DPSCs generated a higher yield of exosomes with improved efficacy in suppressing periodontitis and colitis. The significant upregulation of miR-1246 in 3D culture provided a mechanistic understanding of its superior therapeutic effects, highlighting its role in downregulating Nfat5 and restoring the Th17/Treg balance to treat periodontitis and colitis.

2.1.2 Agitation-based spheroid formation. The agitation-based method requires continuous agitation of cells, through techniques such as shaking, preventing surface adhesion and facilitating cell aggregation for spheroid formation.[49,50] This approach enhances nutrient distribution, facilitates waste removal, and maintains a homogeneous culture environment.[51] However, the mechanical forces generated by agitation can lead to cell damage.[51]

2.1.2.1 Petri dish with gyratory shaker. EVs from human choriocarcinoma (JAr) and endometrial adenocarcinoma (RL95-2) cells were compared between spheroid cultures on a gyratory shaker and conventional 2D monolayer cultures.[52] In both conditions, cells were cultured for 48 hours, then transitioned to serum-free medium for 6 hours before EV collection. EVs were isolated using centrifugation, filtration, and size exclusion chromatography.

Fluorescence-NTA was used to determine the size and concentration of EVs. The 3D culture condition yielded a significantly higher concentration of EVs compared to 2D culture, with a total particle count showing approximately a 1.5-fold increase. The size distribution graph revealed that most EVs from both conditions were primarily in the 100–200 nm size range, with no significant differences in average size between 3D and 2D cultures. Proteomic analysis *via* label-free mass spectrometry revealed distinct differences in the cargo of 2D

and 3D cell-derived EVs. A total of 1313 proteins were detected, with 1204 in 3D-derived EVs and 1159 in 2D-derived EVs. Of these, 1102 proteins were common to both groups, while 102 were unique to 3D-derived EVs and 57 to 2D-derived EVs. Differential expression analysis identified 153 differentially expressed proteins (DEPs) in 3D-derived EVs, with 120 upregulated and 33 downregulated. Pathway analysis revealed that proteins unique to 3D-derived EVs were significantly enriched in cell and focal adhesion, cytoskeleton regulation, and key signaling pathways such as Ras signaling and PI3K-Akt signaling, suggesting that 3D-derived EVs may play a more prominent role in regulating cellular processes like migration, adhesion, and signal transduction. Interestingly, 2D-derived EVs induced a greater stimulation of endometrial epithelial cells (EECs), as evidenced by the increased secretion of Milk fat globule-EGF factor 8 protein (MFGE8) in response to 2D-derived EVs. RL95-2 cells were treated with 2D and 3D JAr-derived EVs for 24 hours, and MFGE8 secretion was measured with ELISA. The results showed higher MFGE8 secretion in cells treated with 2D-derived EVs, indicating that 2D trophoblastic EVs have a stronger impact on EEC signaling compared to 3D-derived EVs.

Overall, the 3D agitation-based spheroid culture produced a higher concentration of EVs with similar sizes to those from 2D culture, enriched proteomic cargo, but demonstrated lower potency in stimulating EEC signaling.

2.1.3 Hanging-drop method. Hanging drop involves placing small droplets of cell suspension upside-down on a lid or flat surface, where gravity and surface tension promote cell aggregation and spheroid formation.[53] By adjusting droplet volume and cell density, spheroid size can be precisely controlled, enabling reproducible formation of uniform aggregates.[43,53,54] This technique is inexpensive, does not require specialized equipment, and is suitable for moderate-throughput applications.[43,54] However, it lacks ECM components and dynamic culture conditions, which may limit physiological relevance. Additionally, media exchange can be technically challenging and labor-intensive, making it less practical for long-term or large-scale studies.[44,55]

The differences in exosome production from BM-MSCs cultured in a 3D hanging-drop (HD) culture system *versus* a monolayer culture were evaluated.[42] BM-MSCs were grown in culture media with 10% exosome-depleted FBS, and exosomes were isolated using a precipitation-based method. Exosome secretion was quantified by measuring exosome protein concentration using a Nanodrop instrument and normalizing to 1×10^5 cells. 3D HD cells secreted significantly more exosomes per cell than 2D cultured cells, with a 2-fold increase observed on day 5 of cell culture ($p < 0.01$). Although exosome production differed significantly between the culture conditions, no other EV properties were assessed.

2.2 Scaffold-based 3D models: hydrogels

Hydrogels are cross-linked polymer networks that retain water and mimic the ECM, providing structural support, biochemical cues, and controlled mass transport for 3D cell culture, unlike scaffold-free models which depend solely on cell–cell interactions.[56] Their low cost, ease of fabrication, and versatility in material composition, including both natural (*e.g.*, collagen, alginate) and synthetic (ex: PEG, PAA) polymers, make them widely used for *in vitro* models.[44] Hydrogels can be tuned for stiffness, porosity, and degradation rate by adjusting parameters like cross-linking density, pH, and temperature, enabling customization for different tissue types.[43,44,57] They also support the diffusion of soluble factors to promote cell growth.[43,44] However, drawbacks include limited mechanical strength, difficulty achieving uniform pore sizes, and reduced suitability for load-bearing tissues.[44]

2.2.1 Collagen. Collagen-based hydrogels are widely used in cancer and tissue engineering models due to their biocompatibility, biodegradability, and ability to mimic the native ECM.[43] As the primary ECM protein, collagen supports cell adhesion, migration, and signaling through cell–matrix interactions, making it particularly relevant for modeling tumor microenvironments.[43,57–59] Its mechanical properties, porosity, and fiber density can be tuned by adjusting parameters such as concentration, pH, temperature, and ionic strength.[43] However, as a natural material of animal origin, collagen poses risks of batch variability and pathogen transmission, and its limited stiffness and stability can restrict its use in long-term or load-bearing applications.[43,44,57]

To simulate the tumor ECM, one study used a collagen-hyaluronic acid (Col1-HA) scaffold to culture Ewing's sarcoma (ES) cells and compared EVs derived from this 3D tissue-engineered (TE) model to those from 2D Col1-HA-coated plates, 3D spheroids in polypropylene tubes, and patient plasma.[60] Cells were cultured for 7 days, and media was collected on days 3 and 7 for exosome isolation using the Total Exosome Isolation Kit from Invitrogen.

Differences in total EV yields between 2D and 3D cultures were not assessed, but NTA analysis revealed a denser distribution of smaller exosomes in the Col1-HA scaffold, resembling patient plasma-derived exosomes (Fig. 4A). The average exosome mode sizes were 103.3 nm (2D culture), 76.7 nm (Col1-HA scaffold), and 70 nm (human plasma), suggesting that 3D structure, scaffold composition, or both influence

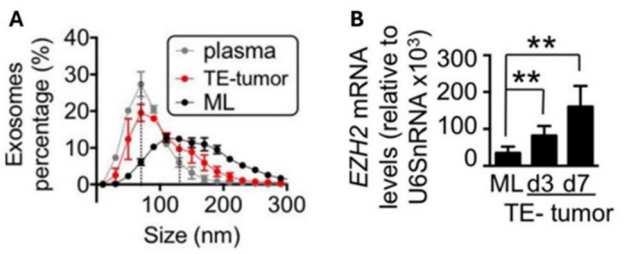

Fig. 4 Characterizing exosomes in tissue-engineered tumours (A) size analysis *via* NTA of exosomes derived from monolayer (ML) culture (n = 3), Col1-HA scaffolds (n = 6), and plasma of ES patients (n = 7). (B) qRT-PCR quantification of EZH2 mRNA in exosomes from monolayer culture and TE tumors on days 3 and 7. Reproduced from ref. 60 with permission from Ivyspring International Publisher, © 2016.

exosome size. Further comparisons with 3D spheroids in polypropylene and monolayer cultures on matrix-coated plates showed that neither system replicated native exosome sizes, emphasizing the necessity of both 3D architecture and matrix composition to mimic physiological exosome characteristics.

The study examined exosomal cargo differences, focusing on Polycomb histone methyltransferase EZH2 mRNA, a key mediator of ES tumor growth and progression. qRT-PCR of RNA from cells and exosomes revealed higher EZH2 mRNA levels in Col1-HA scaffold-derived exosomes compared to those from 2D culture, aligning with levels observed in patient plasma (Fig. 4B). These findings suggest that exosomes from the Col1-HA model could serve as potential ES biomarkers, highlighting their role in EZH2 mRNA enrichment and reinforcing the importance of using native-like experimental models in cancer research. While Western blot analysis revealed an increase in EZH2 protein in Col1-HA TE tumors and undetectable levels in 2D culture, exosomal proteomic cargo was not assessed.

Finally, the study examined the transfer of EZH2 mRNA *via* exosomes from Col1-HA tumor cells to MSCs in the bone niche. After 12 hours, labeled exosomes were internalized by hMSCs, significantly increasing EZH2 mRNA levels compared to untreated hMSCs or those treated with hMSC-derived exosomes. The exosomes also impacted human osteoblasts (hOBs) and osteoclasts (hOCs): while both cell types internalized the exosomes, EZH2 levels remained unchanged in hOBs but decreased in hOCs. These findings demonstrate that EZH2 mRNA-loaded exosomes from Col1-HA scaffolds can transfer to various bone niche cells with distinct effects, though no comparisons were made to 2D cell culture.

ES cells cultured in a collagen-hyaluronate hydrogel produced a denser distribution of smaller exosomes, closely resembling patient plasma-derived exosomes. These exosomes were enriched with EZH2 mRNA, a key marker overexpressed in ES, and they effectively delivered their molecular cargo to various bone niche cells. Supporting this, a study comparing EV production from human oral mucosa lamina propria-progenitor cells (OMLP-PCs) in a collagen-based hydrogel *versus* 2D culture found that 3D culture significantly increased EV concentration.[61] However, the 3D-derived EVs reduced skin fibroblast proliferation relative to 2D-derived EVs, suggesting functional differences driven by the culture environment.

2.2.2 Agarose. Agarose is a natural polysaccharide derived from red algae, valued in biomedical applications for its reversible temperature-sensitive gelation, mechanical stability, and low cytotoxicity.[62] As opposed to collagen which supports cell adhesion, agarose functions as a non-adhesive scaffold that supports spheroid formation by promoting cell–cell interactions and preserving native cell morphology.[62] Its porous structure allows nutrient diffusion, and its properties can be tuned through chemical modification.[62] However, native agarose has limitations, including poor adaptability to complex biological environments, high gelation temperature, and slow degradation, restricting its use in dynamic or long-term systems.[62] To evaluate its utility for EV production, one study compared EVs derived from human gastric cancer (hGC) cells (MKN45 and MKN74) in 2D T175 flasks *versus* agarose hydrogel microwell arrays.[63] In 2D, cells were grown to 60–70% confluence before switching to EV-depleted medium for 48 hours. In 3D, cells were seeded into custom agarose hydrogel microwell arrays, cultured for one day, then maintained in EV-depleted medium for six days. EVs were isolated from the conditioned media of both conditions using differential centrifugation.

EV size and concentration were analyzed using TEM and NTA, showing that 3D-derived EVs were generally smaller (85–135 nm) than those from 2D cultures (100–180 nm). When normalized to cell number, 3D cultures produced significantly more EVs per cell: 1020 EVs per MKN45 cell and 1656 per MKN74 cell, compared to 636 and 365 EVs per cell in 2D, respectively. Imaging flow cytometry confirmed expression of exosome markers CD9, Flotillin-1, and CD81 in both models, with CD9 notably higher in 3D-derived EVs. These findings suggest that hGC cells grown in 3D conditions produce EVs more efficiently while maintaining exosomal marker expression and exhibiting distinct characteristics.

RNA was extracted from cells and EVs using miRNA-specific isolation kits, and qRT-PCR revealed a richer microRNA profile in 3D cultures compared to 2D. A total of 164 miRNAs were found in 3D-derived EVs and 104 in 2D-derived EVs, with 10 exclusively present in 3D-derived EVs and 4 unique to 2D-derived EVs. Overrepresentation analysis of the 10 miRNAs unique to 3D-derived EVs showed significant enrichment in pathways associated with disease states, including lymphoma and inflammatory responses, suggesting their potential roles in these biological processes. Additionally, gene set enrichment analysis of the 164 miRNAs in 3D-derived EVs identified key cancer-associated signaling pathways, including p53, MAPK, TGF-β, and RAS, further underscoring their association with cancer-related mechanisms.

Proteomic analysis of EVs from 2D and 3D cultures using liquid chromatography-tandem mass spectroscopy (LC-MS/MS) identified 430 proteins across both culture conditions. Unsupervised hierarchal clustering revealed that EV origin (MKN45 and MKN74) and culture conditions (2D and 3D) strongly influenced proteomic cargo, forming distinct clusters based on these variables. Supervised clustering of the 20 most differentially expressed proteins between 2D- and 3D-EVs found that 17 of these proteins had decreased expression in 3D-EVs, indicating an overall downregulation of proteins in the 3D condition. Protein set enrichment analysis highlighted significant downregulation of ARF6 signaling pathways in EVs from 3D cultures, suggesting alterations in membrane trafficking and exosome biogenesis.

The association of EVs with recipient cells and their effect on invasion were evaluated. PKH26-labeled EVs from 2D and 3D MKN45 cultures were co-incubated with MCF10A and MKN45 cells for up to 30 minutes. Flow cytometry showed greater uptake of 3D-derived EVs within the first 15 minutes, indicating enhanced early interactions. Invasion assays using Matrigel chambers demonstrated that cells treated with 3D-

derived EVs showed significantly increased invasive capacity compared to those treated with 2D-derived EVs, suggesting a stronger pro-invasive effect.

Cells cultured in agarose hydrogels produced significantly more EVs per cell, which were smaller in size, enriched with cancer-associated miRNAs, and exhibited ARF6 pathway protein downregulation. These EVs also demonstrated stronger recipient cell association and increased invasive potential, highlighting their relevance for EV-based therapeutics and disease modelling. A similar study compared EV production between agarose microwells and monolayer culture, using MSCs from Wharton's jelly of the umbilical cord (UC-MSCs).[64] While a comprehensive analysis of EV yields, genomics, and functionality was not conducted, the study reported similar morphological characteristics and protein numbers between 2D- and 3D-EVs. Notably, 3D-derived EVs were enriched in proteins associated with targeting and localization. Another study using agarose microwells to assess EV production from human adipose-derived stem cells reported increased EV yield and a slight increase in EV size compared to monolayer culture.[65] Spheroid-derived EVs were enriched in wound-healing miRNAs (*e.g.*, miRNA-21-3p) and EV biogenesis genes (*e.g.*, CD82), and demonstrated superior angiogenic and wound-healing effects, achieving the highest degree of wound closure on diabetic rat models.

2.2.3 Peptide. Peptide hydrogels are synthetic, self-assembling materials composed of short peptide sequences that form nanofibrillar networks resembling the ECM.[57,66] Typically assembled through pH- or salt-induced supramolecular interactions, they offer tunable properties ideal for 3D cell culture.[57,66] Commercial formulations like PuraMatrix™, PGmatrix™, and HydroMatrix™ are based on amphiphilic peptides that assemble into β-sheet structures with nanoscale pore sizes, supporting soft tissue applications.[57,66] Their key advantage lies in design flexibility, as mechanical properties, porosity, and bioactivity can be precisely controlled through peptide sequence modifications.[57,66] Unlike natural hydrogels (collagen, agarose, alginate, Matrigel™), peptide hydrogels allow independent tuning of biochemical and mechanical properties, offering greater control and enhancing reproducibility.[57,66] However, they are often expensive, may lack long-term mechanical stability, and are less suited for cultures involving highly contractile cells or large-scale applications.[57] To explore their utility in EV studies, one investigation compared EV production from cervical cancer cells cultured in 2D flasks *versus* 3D peptide hydrogels across multiple time points.[67] For 3D culture, cells were embedded in a peptide PGmatrix™ hydrogel and maintained in 24-well plates. Cells from both conditions were grown in media with 10% exosome-depleted FBS and EVs were collected at defined time points using differential centrifugation and 220 nm filtration, with hydrogel samples mechanically disrupted prior to centrifugation. EV isolation was performed using the Qiagen ExoRNeasy kit for downstream RNA or DNA extraction.

NTA revealed a denser distribution of smaller EVs in 3D cultures compared to 2D (Fig. 5B and D). EVs were collected at 6-hour intervals for 48 hours in 2D cultures and on days 5, 7, 9, 11, and 13 in 3D cultures, showing a three-fold increase in EV secretion by day 9 in 3D cultures, while EV secretion in 2D cultures declined (Fig. 5A and C). qRT-PCR of exosomal and patient plasma RNA showed 96% similarity between 3D-derived EVs and cervical cancer plasma EVs, while 2D cultures

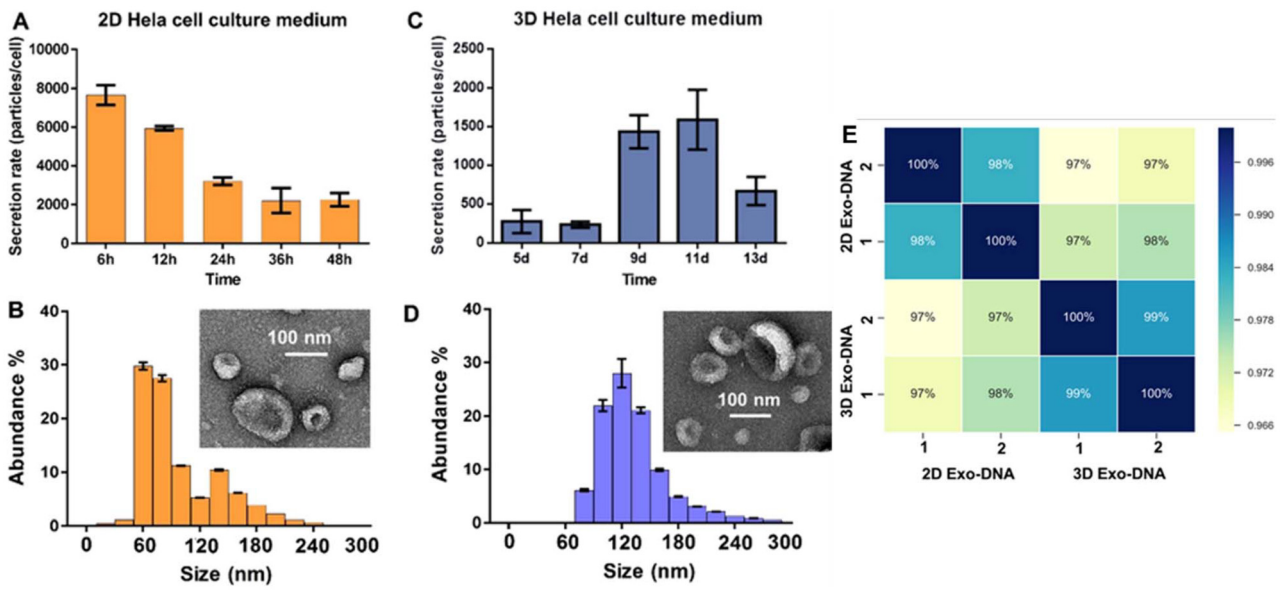

Fig. 5 EV production in 2D cell culture *versus* 3D peptide hydrogel cell culture. NTA comparing the EV secretion rates at timed intervals between 2D (A) and 3D (C) cultures, with live cell counting (n = 3). SEM imaging of EVs from 2D (B) and 3D (D) cultures showed typical cup-shaped morphology (~100 nm). (B & D) EV size and concentration, measured by NTA (n = 5). (E) Spearman correlation matrix of DNAseq reads for 2D- and 3D-derived EV DNA samples. Biological replicates (1 and 2) displayed complete correlation (100%), while 2D- and 3D-derived EV DNA samples demonstrated over 95% similarity. Reproduced from ref. 67 under a Creative Commons Attribution 4.0 International License. © 2019, Springer Nature.

showed only 80% similarity to *in vivo* profiles. Several miRNAs present in 3D culture and patient plasma EVs were absent in 2D-derived EVs, including cancer-related biomarkers. EV DNA analysis *via* Spearman's correlation revealed highly consistent protein-coding gene abundances across EVs in 2D and 3D cultures (Fig. 5E). Non-coding DNA regions analyzed by HOMER showed high similarity between 2D- and 3D-derived EV samples, indicating that EV DNA content remains stable across culture environments.

The peptide hydrogel scaffold produced a denser distribution of smaller EVs, with secretion increasing alongside cell confluency and RNA profiles closely resembling plasma-derived EVs. No differences were observed in EV DNA between the two conditions. Notably, this study is among the few to compare secretion dynamics between the 2D and 3D cultures at multiple time points.

2.2.4 Matrigel™. Matrigel™ is a basement membrane-like membrane material containing ECM components such as collagen IV, laminin, and fibronectin, which undergoes gelation at 37 °C.[68–71] Derived from mouse sarcoma, it is one of the most widely used 3D cell culture platforms due to its ability to support cell differentiation, migration, and organoid formation.[43] Its bioactivity and ease of use make it a standard tool in cancer and developmental biology.[43] However, its animal origin leads to batch-to-batch variability and undefined concentrations of growth factors, which can impact reproducibility and experimental control.[43,57] EVs derived from primary glioblastoma (GBM) cells cultured in 3D Matrigel™ scaffolds were compared to those from 2D culture flasks.[35] 3D cell models were created by embedding GBM cells in Matrigel™ and culturing on an orbital shaker to prevent attachment. Culture supernatants were collected, spun at 200*g* for 5 minutes, and stored at −80 °C. Two different isolation techniques were used to extract EVs from each supernatant sample, precipitation (PP) and immunoaffinity (IA). For IA, the supernatant was centrifuged, vortexed with microbeads, incubated on an overhead rotor, and passed through a magnetic column with multiple washes. EVs were then eluted with isolation buffer. For PP, the supernatant was centrifuged, mixed with a precipitation buffer, incubated at 4 °C, and centrifuged again. The pellet was resuspended in resuspension buffer before storing at −80 °C.

NTA measured EV sizes and concentrations, revealing similar size distribution in EVs from both 2D and 3D cultures for both isolation methods. However, the 3D PP method yielded a significantly higher EV concentration ($6.03 \times 10^8 \pm 1.08 \times 10^8$ particles per mL) than the 2D IA approach ($1.25 \times 10^8 \pm 2.97 \times 10^7$ particles per mL). Flow cytometry confirmed expected tetraspanin enrichment in both 2D- and 3D-derived EVs, with CD81 and CD63 present in ~60% of isolates and CD9 in ~20%. TSG101 was detected in ~90% of PP-isolated EVs from both conditions. Additionally, GBM-related markers CD44 and C1QA were found in ~30% of EVs, with no significant differences between 2D and 3D cultures.

EV RNA was analyzed *via* smallRNA-Seq, showing a higher prevalence of the miRNAs in 3D-derived EVs, regardless of the isolation method. Of the 1964 EV-miRNAs identified, principal component analysis (PCA) clearly distinguished between the 2D and 3D cultures and the two isolation methods. Twelve miRNAs significantly altered in 3D cultures compared to 2D, with nine miRNAs downregulated and three upregulated. Notably, miR-23a-3p, which promotes glioblastoma invasion, was significantly upregulated in 3D, while miR-7-5p, which counters glioblastoma malignancy, was significantly downregulated. Additionally, four miRNAs, miR-323a-3p, miR-382-5p, miR-370-3p, and miR-134-5p, found within the cancer-linked DLK1-DIO3 region, were also identified in 3D EVs. Proteomic analysis of EVs from six GBM models using IA purification and LC-MS/MS identified 462 proteins in 3D-derived EVs, 423 in 2D, with 105 shared. Sixteen proteins were differentially expressed in 3D EVs, and pathway analysis revealed changes in GTPase signaling, immune regulation, and stress response pathways.

Overall, the 3D Matrigel™ scaffold enhances EV secretion from GBM cells, with similar size and marker expression to 2D cultures, while enriching genomic and proteomic cargo associated with critical GBM signaling pathways.

2.2.5 Alginate. Alginate, a plant-derived polysaccharide from brown algae, forms hydrogels *via* ionic crosslinking with divalent ions like calcium.[57] Like agarose, it is biocompatible, non-toxic, and widely used in 3D cell culture to support spheroid formation and maintain rounded cell morphology.[57] Both create non-adhesive, nutrient-permeable environments; however, alginate's ionically crosslinked structure allows easier dissolution and greater versatility in cell encapsulation and recovery, whereas, agarose requires thermal cycling for gelation and dissolution, limiting its compatibility with live cell recovery.[57] Commercial products such as AlgiMatrix™ provide ready-to-use, highly porous alginate scaffolds that support long-term cell viability and enable gentle recovery through chelation.[43,57] Despite this, native alginate lacks cell-adhesive motifs and must be chemically modified (*e.g.*, with RGD peptides) to promote attachment.[57] One EV study compared the production of EVs from BM-MSCs cultured in a coaxially bioprinted alginate hydrogel microfibre to those cultured in a 2D petri dish.[72] The 3D system was created using coaxial extrusion, where a dual-layer coaxial needle simultaneously delivered a cell suspension core and alginate solution shell into a 3% calcium chloride crosslinking pool, inducing rapid gelation and forming hollow, cell-laden microfibres. EVs from 2D and 3D culture were isolated by differential ultracentrifugation from the collected chemical-defined media.

Tunable resistive pulse sensing (TRPS) revealed no significant differences in the sizes of EVs derived from 3D compared to 2D cultures. However, TRPS quantification revealed that the 3D hollow-fibre system enriched EV production by 1009-fold and yielded a ~13-fold increase in EV secretion per cell. Proteomic analysis *via* LC/MS revealed significantly higher proteomic enrichment in 3D exosomes compared to 2D, identifying 1082 high-abundance proteins in EV samples, with 1023 from 3D cultures and 605 from 2D cultures. Of these, 536 proteins were shared (49.1%), while 487 were unique to 3D exo-

somes (44.6%) and 69 unique to 2D exosomes (6.3%). Exosomes derived from 3D cultures were enriched in proteins related to metabolic pathways, ribosome functions, and protein processing. Additionally, EVs from both groups were tested for angiogenic properties using a tube formation assay, where vessel endothelial cells were seeded on Matrigel. Both 2D- and 3D-derived EVs significantly promoted capillary-like network formation, as evidenced by increased branching length and node number.

These findings suggest that the microfiber-based hydrogel not only enhances EV production and proteomic cargo but also preserves angiogenic potential. Supporting these findings, one study used a sodium alginate–hyaluronic acid composite hydrogel and reported a ~3-fold increase in EV production compared to 2D culture.[73] EVs derived from the 3D hydrogel also demonstrated significantly greater therapeutic efficacy than those from 2D cultures, including enhanced cell proliferation and migration, reduced cartilage degradation, and improved cartilage defect repair.

2.3 Scaffold-based 3D models: rigid/fibrous scaffolds

Rigid or fibrous scaffolds, made from natural or synthetic materials, provide superior mechanical strength, stiffness, and wear resistance compared to hydrogels.[37,74] Their interconnected pore and fiber structures influence nutrient diffusion, cellular migration, vascularization, and ECM deposition, making them particularly useful in modeling load-bearing tissues such as bone, cartilage, and muscle.[44,74] Fabrication techniques like electrospinning and 3D printing enable precise customization for specific applications.[74] However, limitations include poor reproducibility with traditional fabrication methods, difficulty achieving uniform pore distribution, and limited suitability for soft tissue applications.[44] Moreover, some rigid scaffolds may hinder deep cellular infiltration or introduce stress conditions that affect cell behavior and EV cargo composition.[44]

2.3.1 Synthetic scaffolds. A study explored how the architecture and surface composition of 3D-printed scaffolds influence the therapeutic potential of osteoblast-derived EVs for bone repair, in comparison to 2D cultures.[75] Titanium scaffolds with triangular (T) or square (S) shapes and pore sizes of 500 μm (500) or 1000 μm (1000) were created using selective laser melting and coated with nano-needle hydroxyapatite (nnHA). MC3T3 pre-osteoblasts (pre-OBs) and BM-MSCs were seeded on the scaffolds (2×10^5 cells per scaffold), cultured dynamically at 8 rpm, and incubated in osteogenic medium. EVs were isolated from 14-day cultures by differential centrifugation, washed, and resuspended in PBS for further analysis.

Isolated EVs were analyzed using TEM, which confirmed their spherical morphology, consistent across scaffold- and 2D-cultured osteoblast-derived EVs. EV size distribution was measured by Dynamic Light Scattering (DLS), showing an average diameter of ~200 nm, though size differences between culture models were not calculated (Fig. 6A). Total EV protein concentration was measured using a BCA assay, while ELISA quantified CD63-positive particles, an EV-specific marker. Both values were normalized to cell number. EVs from both culture systems expressed positive EV surface markers, but ELISA revealed an over 3.4-fold increase in CD63-positive particles from scaffold cultures compared to the 2D cultures (Fig. 6B). Similarly, scaffold-derived EVs showed a significant increase in protein content (over 1.32-fold, $P \leq 0.01$) relative to 2D-derived EVs (Fig. 6C). Among the 3D culture variants, T1000 scaffolds produced the highest EV yields (CD63+ particles) with the most enhanced protein content.

Intracellular calcium content, known to influence EV biogenesis, was measured using a calcium colorimetric assay kit and found to be significantly higher in scaffold-cultured cells compared to 2D-cultured cells (over 9.1-fold, $P \leq 0.001$) (Fig. 6D), with the T100 scaffold showing the highest levels. The osteogenic potency of scaffold-derived EVs was assessed by measuring alkaline phosphatase (ALP) activity in BM-MSCs. Significant increases in ALP activity were observed in EVs from 3D scaffolds compared to 2D cultures, except for the S1000 model, with T500-EVs inducing the highest ALP activity (Fig. 6E). Additionally, scaffold-derived EVs were evaluated for their impact on extracellular matrix formation and mineralization in BM-MSCs by measuring collagen production and calcium deposition. While overall differences between 2D and 3D cultures were not statistically significant, individual 3D models showed notable variation, with T500-EVs driving the greatest increases in both collagen levels (Fig. 6F) and calcium deposition (Fig. 6G). Lastly, the effects of the nnHA coating on EV production were assessed by comparing uncoated and nnHA-coated scaffolds. The coating resulted in a 2.6-fold increase in osteoblast mineralization and a 4.5-fold increase in EV production ($P \leq 0.001$). This enhancement is likely due to elevated intracellular calcium levels and a more biomimetic microenvironment, both of which promote vesicle secretion.

This study compared 2D and 3D cell cultures while also investigating variations among different 3D scaffolds, highlighting how scaffold properties influence EV production. Overall, the rigid 3D scaffold enhanced EV yield, enriched protein content, and improved the osteogenic potential of EVs, including their ability to promote osteoblast mineralization. Triangular pore designs demonstrated the most significant enhancements, and while the ideal pore size for EV production remains uncertain, larger pores (1000 μm) notably increased EV yields.

Another study using 3D-printed hydroxyapatite scaffolds investigated differences in EV production from human umbilical vein endothelial cells (HUVECs) cultured on 3D scaffolds *versus* 2D culture.[76] The findings revealed that the 3D-cultured EV group exhibited higher EV yields as demonstrated through enhanced exosome marker expression, elevated VEGF and CD31 mRNA and protein levels, and superior proliferative, migratory, and angiogenic effects.

2.3.2 Natural scaffolds. The impact of BM-MSC derived exosomes from collagen scaffolds (3D-Exos) *versus* monolayer culture flasks (2D-Exos) on spatial learning in traumatic brain

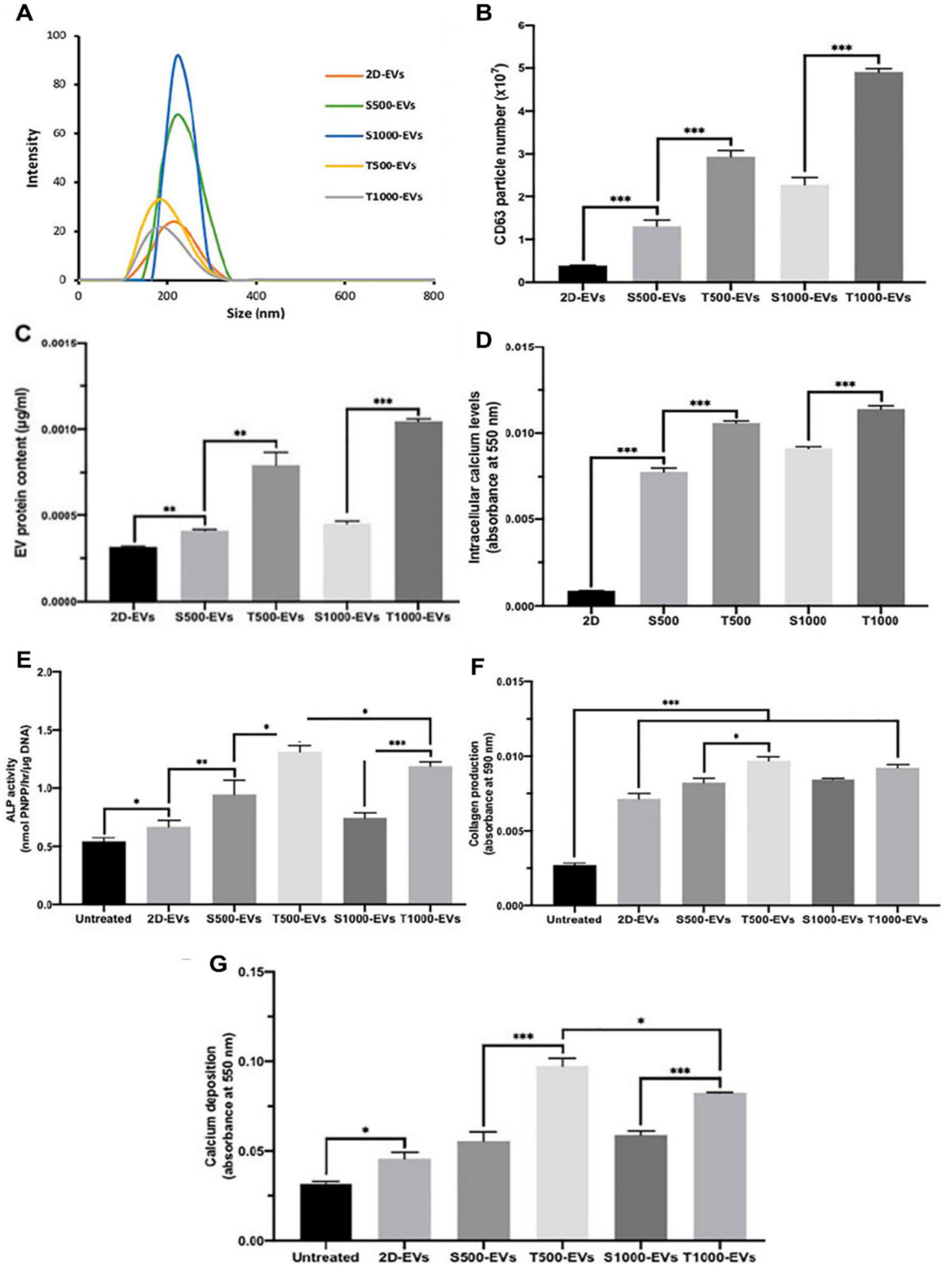

Fig. 6 EV characterization from 2D cell culture and 3D titanium scaffold variants. (A) EV size distribution. (B) Quantification of CD63+ particles. (C) Protein content of EVs. (D) Intracellular calcium content. (E) Alkaline phosphatase (ALP) activity in BM-MSCs treated with EVs. (F) Collagen production in BM-MSCs following EV treatment. (G) Calcium deposition in BM-MSCs treated with EVs after 21 days in osteogenic culture. Data presented as mean ± SD (n = 3). $^{**}P \leq 0.01$ and $^{***}P \leq 0.001$. Reproduced from ref. 75 under a Creative Commons Attribution 4.0 International License. © 2021, Frontiers.

injury (TBI) rat models was investigated.[77] The 3D scaffold consisted of Ultrafoam scaffolds which were fabricated by cutting sterile, commercially sourced collagen type I hemostatic sponges (Avitene Ultrafoam) into 5 mm diameter, ~5 mm thick discs. These porous, water-insoluble scaffolds are derived from purified bovine corium collagen treated with hydrochloric acid. After cells in both conditions reached 60–80% confluence, the conventional culture media was replaced with media containing exosome-depleted FBS. The cells were then cultured for 48 hours before collecting the media for exosome isolation. Exosomes were isolated using the ExoQuick-TC protocol, which involves incubating the collected media with the reagent for 12 hours, followed by centrifugation to pellet the exosomes.

While this study did not characterize the exosomes in terms of yield, size, or genomic cargo, they did assess the EV protein content and execute several *in vivo* functionality tests on TBI rat models. Using the BCA assay, it was found that the 3D scaffold produced approximately twice the amount of exosomal protein compared to 2D culture (168.5 ± 11.2 μg *vs.* 84.7 ± 5.5 μg, $p < 0.05$). Functional outcomes were evaluated using a modified Morris Water Maze (MWM) test on days 31–35 post-injury. Rats treated with 3D-Exos demonstrated significantly improved spatial learning, spending more time in the target quadrant and locating the hidden platform faster than those in the Exo-2D and liposome-treated groups ($p < 0.05$). Beyond cognitive improvements, the Exo-3D group also exhibited increased numbers of newborn mature neurons in the dentate gyrus and reduced neuroinflammation, as shown by lower levels of reactive astrocytes and activated microglia. These findings underscore the enhanced therapeutic potential of 3D-derived exosomes for promoting both cognitive recovery and neural repair after TBI.

Another study using a natural fibrous scaffold examined how silk fibroin woven scaffolds affected the cargo and functionality of exosomes derived from human dermal microvascular endothelial cells (HDMVECs).[78] Compared to 2D cultures, exosomes from the 3D scaffold carried significantly higher levels of angiogenic factors, including IL-1α, angiopoietin-1 and -2, MMP-1, and uPAR. Functionally, these 3D-derived exosomes more effectively promoted tube formation by HDMVECs *in vitro*, demonstrating enhanced pro-angiogenic potential. Together, these studies support the use of natural fibrous scaffolds to enrich EV proteomic content and improve their functional bioactivity.

2.4 Scaffold-based 3D models: bioreactors

Contrary to the previous static 3D platforms, bioreactors are dynamic 3D culture systems that provide an optimal and controlled environment, through techniques such as perfusion, wave-motion, stirred tanks, and vertical wheels.[37] These systems can also incorporate microcarriers into the culture.[79,80] Bioreactors offer key advantages such as enhanced standardization and reproducibility, scalability for large-scale cell expansion, and precise control over experimental conditions to study cellular responses.[81] The drawbacks of using these systems include the high cost, complexity of the equipment, and flow limitations such as shear stress.[82]

2.4.1 Perfusion systems. In perfusion systems, cells within the bioreactor are continuously fed with fresh medium, eliminating waste and depleted medium, while ensuring a constant supply of nutrients and carbon sources.[83] This approach offers several benefits, including limited turbulence, a compact setup, and potential for automation.[81] However, shear forces from continuous flow may impact cell viability and differentiation, which must be carefully managed depending on the application.[81]

2.4.1.1 Hollow-fibre bioreactor. Hollow-fibre bioreactors feature semi-permeable fibres bundled in a tubular shell, allowing cells to grow on the outside while media continuously flows through the fibre lumen.[37] One study compared EV production from UC-MSCs cultured in a hollow-fibre bioreactor *versus* 2D flasks and assessed their impact on acute myocardial infarction (AMI).[84] UC-MSCs were grown in culture media with 10% FBS. For 2D culture, passage 6 cells were plated in T75 flasks. For 3D culture, cells were seeded in the external space of a FiberCell hollow-fibre bioreactor. After 24 hours, the medium was replaced with EV-depleted medium in both systems. Glucose levels were monitored in the bioreactor and medium was refreshed upon a 50% drop. EVs were collected after 48 hours of culture in EV-depleted medium, isolated *via* sequential centrifugation, filtration, and ultracentrifugation, and further purified with a wash and a second ultracentrifugation.

NTA and TEM revealed no significant differences in EV sizes from 2D (139.2 nm) and 3D cultures (135 nm), but NTA showed that 3D culture-derived EVs had a significantly higher nanoparticle count per volume. Over 30 days, 3D culture yielded 8.21 times more EVs than 2D from the same cell media volume. Functional studies demonstrated that 3D culture-derived EVs had enhanced cardioprotective effects both *in vitro* and *in vivo*. In rat H9c2 cells subjected to hypoxia, EVs from the bioreactor significantly reduced apoptosis, as indicated by lower percentages of apoptotic cells and reduced caspase 3/7 and propidium iodide (PI)-positive staining detected by flow cytometry. Additionally, EVs from 3D culture promoted increased angiogenesis in hypoxic HUVECs, evidenced by greater tubular structure formation. Anti-inflammatory effects were also more pronounced with 3D cultured EVs, which reduced inflammatory cytokines like TNF-α and IL-1β, as well as iNOS expression in LPS-stimulated RAW264.7 cells. In a rat AMI model, treatment with the bioreactor-produced EVs significantly reduced infarct area, improved left ventricular ejection fraction (LVEF) and fractional shortening (LVFS), and enhanced overall cardiac function compared to EVs from 2D culture. These findings suggest that 3D-EVs provide superior cardioprotective effects and improve cardiac function post-AMI.

This hollow-fibre bioreactor system enhanced EV production, yielding sizes comparable to those from 2D culture, and significantly improved cardioprotective effects both *in vitro* and *in vivo*. Supporting this, two other studies comparing EV secretion from hollow-fibre bioreactors to monolayer cultures using UC-MSCs also found increased EV secretion,

with no significant differences in size, alongside enhanced functional effects, such as improved anti-inflammatory activity.[85,86] Furthermore, a study comparing HEK293-derived EVs from 3D hollow-fibre bioreactors and 2D cultures reported significantly higher EV secretion with similar EV sizes between the two conditions.[87]

2.4.1.2 3D-printed scaffold perfusion bioreactor. EV production from human dermal microvascular endothelial cells (HMDECs) was compared across a 3D-printed scaffold perfusion bioreactor system, a static scaffold, and a 2D system.[88] The scaffold, printed from a biocompatible acrylate material, was designed to enhance nutrient and gas exchange. Cells were seeded onto gelatin-coated scaffolds for both the dynamic perfusion and static conditions and cultured into T75 flasks for the 2D condition. EVs were collected from the conditioned media of all three conditions after 24 and 48 hours, and isolated using differential centrifugation followed by passage through a sterile 0.2μm filter.

NTA revealed that the size distributions of EVs were similar across all three culture conditions and remained consistent between both collection time points, with 90% of EVs between 40–200 nm. NTA also demonstrated a significant increase in EV production in the bioreactor culture, with an approximately 100-fold increase on day 1 ($p < 0.0001$) and a 10 000-fold increase on day 3 ($p < 0.0001$) compared to both the static scaffold and flask controls. CD63 ExoELISA further confirmed the enhanced EV production in the bioreactor culture compared to the flask, though only a ~14-fold increase was observed. Protein quantification by BCA assay showed that total EV yield in the Bioreactor (~1000 μg) was significantly higher than the flask (~150 μg) and scaffold (~400 μg) cultures at both collection time points. However, protein content per EV was inversely correlated with EV production rates, as Day 1 and 3 bioreactor-derived EVs exhibited more than 15-fold ($p < 0.001$) and 70-fold ($p < 0.001$) reductions in total protein content per EV, respectively, compared to 2D culture. An *in vitro* gap closure assay was also conducted to evaluate the bioactivity of HMDEC-derived EVs by measuring endothelial cell migration following the introduction of a gap in the monolayer using a pipette tip. The results indicated no significant difference in gap closure between HDMECs treated with basal media alone and those treated with EVs from any culture condition.

These results suggest that the dynamic culture conditions of this perfusion scaffold bioreactor enhance EV yields, producing vesicles of similar size to those derived from 2D culture. However, the protein content appears compromised, and no significant differences in wound healing effects were observed in the EV-treated HMDECs. Similarly, a study comparing MSC-derived EVs from a 3D-printed scaffold perfusion bioreactor and conventional 2D culture reported a ~40–80-fold increase in EV production, with comparable EV morphology and size.[89] While protein content per EV was also reduced in this study, a wounded mouse model, showed that EVs from the perfusion bioreactor significantly enhanced wound healing compared to 2D-derived EVs. A third study further supported these results, demonstrating a 67-fold increase in EVs per cell and a 2.14-fold reduction in protein per EV, while preserving biological function through enhanced fibroblast and keratinocyte migration.[90]

2.4.2 Wave-motion bioreactor. Wave-motion bioreactors use a rocking motion to create waves that agitate and gently mix the cell culture media, facilitating effective oxygenation and nutrient transfer, while minimizing shear stress.[91,92] They are compatible with versatile single-use bags, which simplify setup and reduce contamination risk.[81] However, their limited scale-up potential may restrict use in large-manufacturing applications.[81] The impact of a wave bioreactor *versus* 2D cell culture on BM-MSC derived EVs (MSC-EVs) was investigated.[93] To prepare 3D cell cultures, cells were seeded in ULA 6-well plates and cultured dynamically on a rocking platform in a wave bioreactor under controlled shear stress to form aggregates (100–300 μm diameter) over 18–72 hours. For EV collection, the culture media was replaced with EV-depleted FBS media and incubated for 2 days. The conditioned media was collected, and EVs were isolated *via* ultracentrifugation and polyethylene glycol (PEG) precipitation, followed by resuspension in PBS and a final centrifugation at 10 000*g* before storage at −80 °C.

NTA measured the size distribution and particle concentration of EVs, revealing that 3D culture produced two-fold more EVs per cell than 2D culture (Fig. 7A), with smaller mode sizes for 3D (100 nm) compared to 2D (155 nm). TEM confirmed the morphology and size distribution, showing smaller average sizes for 3D-MSC-EVs (55 nm) compared to 2D-MSC-EVs (75 nm) and the presence of exosome-like vesicles (Fig. 7B and C). Western blot analysis detected higher levels of exosomal markers, including Alix, Flotillin-2, CD81, and CD63, in 3D-MSC-EVs. miRNA profiling indicated significant upregulation of miR-21-5p (26-fold), miR-1246 (5.2-fold), and miR-22-3p (2.5-fold) in 3D-MSC-EVs (Fig. 7D). LC/MS identified 1254 shared proteins, with 102 unique to 3D-MSC-EVs and 6 unique to 2D-MSC-EVs (Fig. 7E). Differentially expressed protein (DEP) analysis showed 618 upregulated proteins (49.3%) in 3D-MSC-EVs compared to 122 (9.7%) in 2D-MSC-EVs, with enrichment in pathways related to cell adhesion, extracellular matrix (ECM) interactions, and neurodegenerative diseases. Notably, the total protein content per 10^8 EVs was significantly lower in 3D-derived EVs compared to 2D-derived EVs (Fig. 7F), likely reflecting the smaller size of EVs in the 3D group.

This study also compared the immunomodulatory, wound healing, and anti-senescence effects of EVs derived from 2D- and 3D-cultured hMSCs, revealing distinct functional properties. Both EV types reduced pro-inflammatory cytokines (TNF-α, IL-6, IL-12β) in LPS-stimulated macrophages, but neither induced clear M1/M2 polarization, as confirmed by mRNA profiling (Fig. 7G). 2D-hMSC-EVs elicited a greater increase in indoleamine 2,3-dioxygenase (IDO) activity in IFN-γ-licensed hMSCs (14.3-fold) compared to 3D-hMSC-EVs (8.5-fold) and the untreated control (5.9-fold), indicating stronger immunomodulatory potential in this assay. However, 3D-hMSC-EVs more significantly suppressed CD8+ and CD4+ T cell proliferation and enhanced wound healing (Fig. 7H),

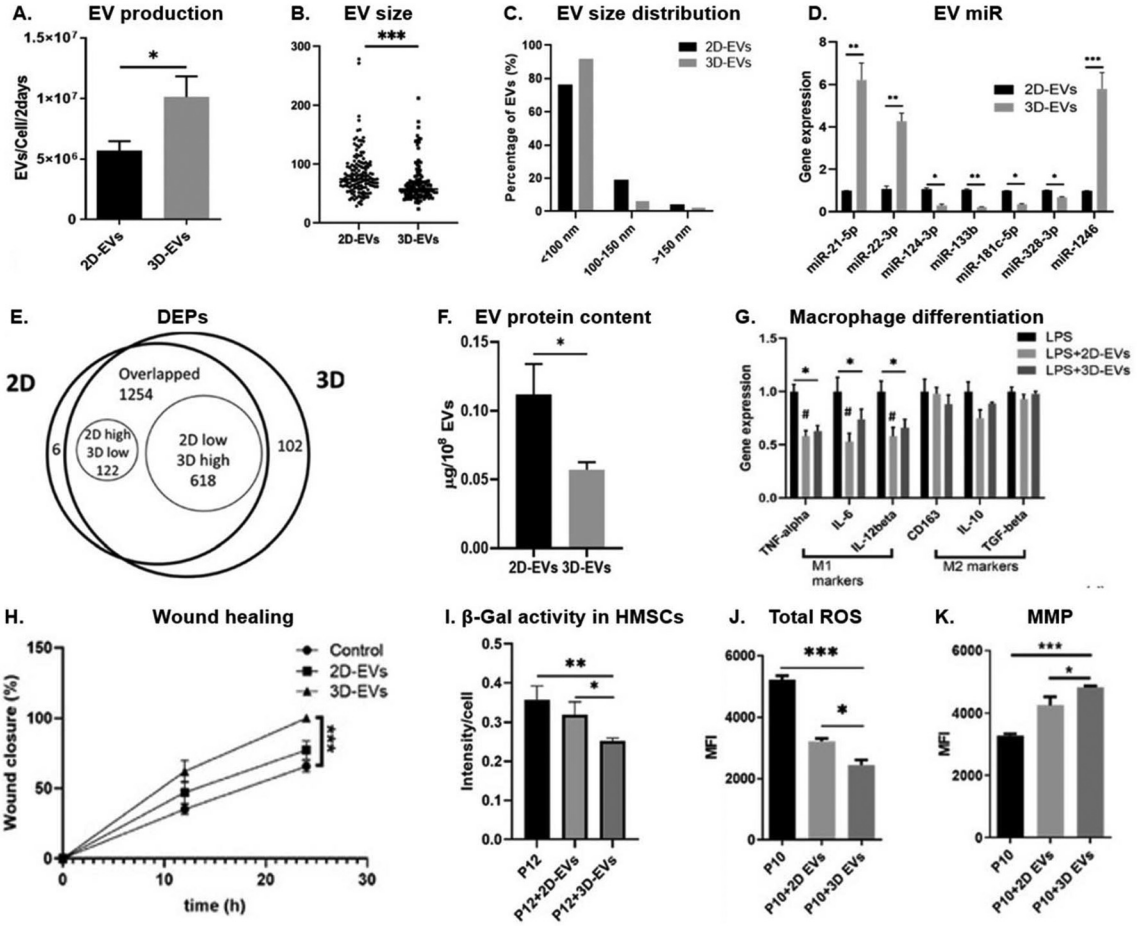

Fig. 7 Properties and functionality of MSC-derived EVs from 2D and 3D cell culture (A) EV production rates per cell in 2D and 3D cultures over two days, measured *via* NTA (n = 6). (B) EV size (n = 150) and (C) size distribution analyzed from TEM imaging. (D) miRNA expression levels in EVs quantified by qRT-PCR (n = 3). (E) Total protein content in EVs (n = 3). (F) Venn diagram of differentially expressed proteins (DEPs) in 2D *versus* 3D-EVs based on LC/MS proteomic analysis. (G) Expression of M1 and M2 macrophage markers following LPS stimulation and EV treatment (n = 3). (H) Percentage of wound closure in human fibroblasts after EV treatment (n = 3). (I) β-Galactosidase (β-Gal) activity in senescent MSCs (P12) treated with EVs (n = 3). (J) Reactive oxygen species (ROS) levels n BM-MSCs after EV treatment. (K) Mitochondrial membrane potential (MMP) in senescent MSCs (P10) evaluated with flow cytometry after EV treatment (n = 3). *P < 0.05; **P < 0.01; ***P < 0.001. Reproduced from ref. 93 under a Creative Commons Attribution 4.0 International License. © 2022, John Wiley & Sons, Inc.

reduced senescence (lower β-Gal activity) (Fig. 7I), decreased ROS levels (Fig. 7J), and maintained mitochondrial fitness in higher-passage hMSCs (Fig. 7K). These effects correlated with distinct molecular cargo differences identified through multi-omics analysis, including increased miRNA-21 levels, LDL-associated proteins (*e.g.*, APOE, HDLBP), and ROS-scavenging proteins.

The wave motion bioreactor cultures cells that enhance EV production, generating EVs with superior cargo and functional properties, particularly for immunomodulation, tissue repair, and anti-aging therapies.

2.4.3 Microcarrier-based bioreactors. Microcarriers are small spherical beads (100–300 μm) that serve as scaffolds for adherent cells, allowing their attachment and growth in suspension-based dynamic systems like bioreactors.[37,94] They can be made from synthetic or natural materials, and vary in porosity and surface properties, such as charge, hydrophilicity, and ECM coatings.[37,94] Solid microcarriers support adherence and expansion of cells, while microporous types, offer protection from shear forces in the bioreactor system, such as stirred-tank cultures.[95] However, these porous microcarriers may present diffusion limitations for nutrients and oxygen, potentially leading to necrotic regions in cells deep within the microcarrier.[95]

2.4.3.1 Microcarriers in a vertical wheel bioreactor. A vertical wheel bioreactor features a vertically oriented impeller wheel within a chamber that generates controlled mixing, promoting uniform hydrodynamic forces.[96,97] This design ensures an even distribution of nutrients, gases, and cells, while minimizing turbulence and shear stress.[96,97] Such conditions are optimal for cell aggregation, leading to efficient spheroid formation.[97] A study compared EVs secreted from BM-MSCs cultured on microcarriers in a vertical wheel bioreactor to those from conventional 2D flasks.[80] BM-MSCs, initially grown in 2D

to 80% confluence, were seeded statically onto Synthemax II Microcarriers in the bioreactor at 4600 cells per cm^2. After adhesion, the bioreactor rotation was set at 25 rpm, increased to 35 rpm after 72 hours, and media was replenished. On day 5, collection media was added, and EVs were harvested after 72 hours. Cells and media were processed to isolate EVs using ultracentrifugation, with the final EV sample resuspended in PBS and stored at −80 °C.

NTA revealed similar EV size distributions between 2D and 3D cultures, with average diameters of 139.13 nm and 146.86 nm, respectively. While not statistically significant due to limited replicates (n = 4), 3D cultures produced 28 times more EVs per mL than 2D. ExoView analysis showed significantly higher expression of CD81 and CD9 in 3D culture-derived EVs. 3D cultures yielded 6.47×10^8 $CD81^+$ and 2.17×10^8 $CD9^+$ particles per mL, compared to 3.67×10^7 and 3.09×10^7 in 2D, respectively. 3D-EVs also exhibited higher tetraspanin copy numbers and more triple-positive exosomes, indicating greater molecular diversity and protein enrichment.

To assess neuroregenerative effects, trigeminal ganglia (TG) neurons were treated with EVs from 2D and 3D cultures. After five days, neurons were stained for β3-tubulin and imaged *via* confocal microscopy. Neurite growth was quantified using Neurolucida software. Compared to 2D-EVs, 3D-EVs significantly enhanced neurite elongation (3301.5 μm *vs.* 1860.5 μm, $P < 0.05$) and complexity, with Sholl analysis showing a seven-fold increase in total neurite length (14 588.2 μm *vs.* 2243.96 μm, $P < 0.05$). Bright-field imaging also revealed more extensive neurite sprouting in 3D-EV-treated cultures.

The microcarriers in the vertical wheel bioreactor promote increased secretion of EVs with enhanced surface marker expression and neuroregenerative properties. These findings underscore the superior neuroregenerative potential of microcarrier-produced EVs.

2.4.3.2 Microcarriers in a stirring spinner flask. Spinner flasks are cylindrical vessels designed for suspension-based cell culture, providing gas exchange through side arms with loose screw caps and mixing *via* a non-suspended magnetic stir bar.[98] A study compared EV production from UC-MSCs cultured on Star-Plus microcarriers in spinner flasks *versus* conventional 2D flasks, while also evaluating two EV isolation methods, tangential flow filtration (TFF) and ultracentrifugation (UC).[79] Cells were seeded at a density of 8000 cells per cm^2 on 3.2 g of microcarriers in 250 mL flasks stirred at 36 rpm. A pump circulated the medium through membranes with specific pore sizes to selectively remove smaller particles while retaining larger particles in the system. After cell attachment, cultures were switched to serum-free, xeno-free medium. For TFF, conditioned media were filtered through a 200 nm membrane to eliminate large vesicles and particles, concentrated 9 times using 500 kDa size exclusion hollow fiber filter, and continuously replenished with PBS to compensate for volume loss before sterile filtration, yielding exosomes suspended in PBS.

NTA and TEM confirmed similar size distributions of exosomes across all groups, regardless of culture or isolation method. However, yields differed significantly. Using conventional UC, 3D cultures produced 20 times more exosomes than 2D and combining 3D culture with TFF further increased yield 7-fold, resulting in a 140-fold total exosome yield increase over the 2D UC method. Additionally, Bradford protein assays revealed that exosomes from 3D cultures had 2–4 times more proteins per vesicle compared to those from 2D ($P < 0.0001$). Specifically, 3D-UC and 3D-TFF exosomes had 0.9×10^9 and 1.23×10^9 particles per mg of protein, compared to 2.6×10^9 and 4.0×10^9 for 2D-UC and 2D-TFF, respectively, suggesting higher protein content per vesicle in 3D-derived samples.

To assess exosome functionality, cortical neurons were incubated with siRNA-loaded exosomes from all conditions for 7 days to evaluate Huntingtin gene silencing. Huntingtin mRNA levels were measured using the QuantiGene 2.0 assay kit and normalized to Hprt. 3D-TFF-exosomes were 5 times more effective at transferring siRNA and silencing Huntingtin in neurons than 2D-UC-exosomes ($p < 0.0001$), while no significant differences were observed among 3D-UC-exosomes, 2D-TFF-exosomes, and 2D-UC-exosomes. To examine vesicle uptake, neurons were treated with fluorescently labeled siRNA-loaded exosomes from each condition. Neurons absorbed significantly more fluorescent siRNA-loaded 3D-TFF- and 3D-UC-exosomes than 2D-UC- and 2D-TFF-exosomes ($p < 0.0001$). This indicates that the culture conditions of the parent cells significantly influence exosome uptake by neurons. While vesicle uptake alone does not directly account for Huntingtin silencing efficacy, the enhanced uptake of 3D-TFF-exosomes likely contributes to their superior performance in silencing Huntingtin.

The microcarriers in a stirring spinner flask significantly increased EV yields and favoured the production of protein-dense vesicles. Incorporating the TFF isolation method further amplified these effects and enhanced EV uptake by recipient cells compared to other conditions, potentially improving therapeutic efficacy.

2.5 Summary of 3D cell culture models and their impact on EVs

Table 1 provides a summary of recent 3D cell culture models, detailing key aspects such as the subtype (*e.g.* spheroids), platform (*e.g.* non-adherent 96-well plates), cell line, and their impact on EVs compared to 2D cell culture, including EV yield, morphology, genomic and proteomic analysis, and functionality. Most 3D models demonstrate higher EV concentrations with enriched molecular cargo and enhanced functionality, underscoring their capacity to better mimic *in vivo* conditions and their potential utility in diagnostic and therapeutic application.

3. Discussion & future perspectives

This review has explored recent studies comparing 3D cell culture models with conventional 2D cultures, focusing on their effects on EV production and properties. Across these studies, almost all reported a significant increase in EV concentrations when employing 3D

Table 1 Summary of the results from studies investigating the impact of 2D *versus* 3D cell culture models on EVs

Application		Impact of 3D cell culture on EVs compared to 2D					Ref.
Platform	Cell line	Yield	Morphology	Genomic analysis	Proteomic analysis	Functionality	
Spheroids							
Non-adherent 96-well plates	BM-MSCs	NSD[a]	NSD	N/A[a]	Similar protein yield Fewer and less functionally diverse proteins	Reduced anti-inflammatory, anti-fibrotic, & macrophagic activity	46
	PANC-1	Increased	N/A	miRNA enrichment	Increased GPC-1 protein	N/A	45
	BM-MSCs	Increased	N/A	N/A	N/A	N/A	42
ULA culture dish	DPSCs	Increased	N/A	miRNA enrichment	N/A	Improved therapeutic effects on periodontitis and colitis	48
Petri dish with gyratory shaker	JAr & RL95-2	Increased	NSD in size/ shape	N/A	Protein enrichment: enriched in adhesion, plasma membrane localization, & migration proteins	Greater endometrial epithelial cell stimulation by 2D-derived EVs (increased MFGE8 secretion)	52
Hanging drop	BM-MSCs	Increased	N/A	N/A	N/A	N/A	42
Hydrogels							
Agarose	hGC cells	Increased	Smaller	miRNA enrichment; significantly enriched in disease-related pathways	Significant downregulation of ARF6 signaling pathway proteins	Enhanced invasion capacity of recipient cells	63
	UC-MSCs	N/A	Similar size	N/A	Similar protein number Enriched in targeting/localization proteins	N/A	64
	hASCs	Increased	Slightly larger size	Enriched in wound-healing miRNAs and EV biogenesis genes	N/A	Enhanced angiogenic wound healing properties	65
Collagen	ES cells	N/A	Smaller	Increased EZH2 mRNA	N/A	N/A	60
	OMLP-PCs	Increased	NSD in modal size	N/A	N/A	Significantly reduced skin fibroblast proliferation	61
Peptide	Cervical cancer HeLa cells	Increased	Smaller	RNA profile more *in vivo*-like Similar DNA	N/A	N/A	67
Matrigel	Primary GBM cells	Increased	Similar	miRNA enrichment, more *in vivo*-like	Enriched motility, immune regulation, & ECM proteins	N/A	35
Alginate	BM-MSCs	Increased	NSD in size	N/A	Protein enrichment	Comparable angiogenic abilities to 2D	72
	UC-MSCs	Increased	NSD in size	N/A	N/A	Improved proliferation and migration of cells, suppression of cartilage degradation, and improved efficacy in cartilage defect repair	73
Rigid/Fibrous Scaffolds							
Titanium scaffold with hydroxyapatite	Pre-OBs & BM-MSCs	Increased	Similar	N/A	Increased protein content	Enhanced osteogenic potential	75
3D-printed hydroxyapatite scaffold	HUVECs	Increased	N/A	Increased VEGF & CD31 mRNA expression	Increased VEGF & CD31 protein expression	Superior proliferative, migratory, and angiogenic effects	76
Collagen scaffold	BM-MSCs	N/A	N/A	N/A	Increased protein content	Enhanced spatial learning when injected into TBI rat	77
Silk fibroin woven scaffold	HDMVECs	N/A	N/A	N/A	Increased angiogenic growth factors	Increased tube formation via induction of HDMVECs	78
Microcarriers & Bioreactors							
Perfusion scaffold	HDMECs	Increased	Similar size	N/A	Reduced protein per EV	NSD in gap closure effect on HMDECs	88
	MSCs	Increased	NSD	N/A	Reduced protein per EV	Maintained angiogenic bioactivity and enhanced wound healing	89
		Increased	N/A	N/A	Reduced protein per EV	Maintained pro-angiogenic activity and wound healing	90

Table 1 *(Contd.)*

Application		Impact of 3D cell culture on EVs compared to 2D					Ref.
Platform	Cell line	Yield	Morphology	Genomic analysis	Proteomic analysis	Functionality	
Hollow fibre	HEK293	Increased	Similar size	N/A	N/A	N/A	87
	UC-MSCs	Increased	NSD	N/A	NSD in surface markers	Enhanced renoprotective, anti-inflammatory, and therapeutic efficacy	85
		Increased	N/A	N/A	N/A	Enhanced proliferative, migratory, and matrix-synthesizing effects with improved chondrocyte stability	86
		Increased	Similar	N/A	N/A	Enhanced cardioprotective efficacy	84
Wave-motion bioreactor on ULA plates	BM-MSCs	Increased	Smaller	miRNA enrichment	Reduced protein per EV Increased upregulation of specific DEPs	Improved immunomodulation & rejuvenation of senescent cells	93
Microcarriers in a vertical wheel	BM-MSCs	Increased	Similar size	N/A	Enriched in CD9, CD81, CD63	Enhanced neuroregenerative properties	80
Microcarriers in stirring spinner flask	UC-MSCs	Increased	Similar size	N/A	Increased protein per EV	Improved siRNA transfer & Huntingtin silencing	79

[a] Acronyms used: NSD: no significant differences; NA: not applicable – parameter was not investigated.

cultures.[35,42,45,48,52,61,63,65,67,72,73,75,76,79,80,84–90,93] However, one exception involved a study using non-adherent 96-well plates to form spheroids, where no significant differences in EV yields were observed.[46] This was likely due to limited EV release from cells deep within the spheroids, attributed to high cell density and increased spheroid size.[46] Supporting this, another study reported a rapid decrease in exosome secretion with increasing cell density and spheroid size.[42] These findings suggest that cell density and spheroid dimensions are critical parameters for optimizing EV production.

Over half of the reviewed studies observed similar EV morphology between 2D and 3D cultures.[35,46,52,61,64,72,73,75,79,80,84,85,87–89] However, some reported that 3D-derived EVs were smaller and closer in size to native EVs.[60,63,67,93] Notably, studies involving collagen hydrogel,[60] agarose hydrogel,[63] peptide hydrogel,[67] and wave motion bioreactors reported such size differences,[93] highlighting the influence of ECM components and dynamic culture conditions on *in vivo*-like EV production. One study using agarose microwell culture found that EVs produced in 3D were slightly larger than those from 2D culture.[65] However, it was the only study reviewed that used human adipose-derived stem cells, suggesting that the observed increase in EV size may reflect a cell-type-specific secretory adaptation. As such, these findings may not be generalizable to other cell types or 3D culture platforms.

Genomic analysis from multiple studies revealed that 3D-derived EVs had richer mRNA and miRNA profiles compared to their 2D counterparts.[35,45,48,60,63,65,67,76,93] These enriched profiles included upregulation of specific disease-related pathways, which could enhance understanding of disease mechanisms and improve diagnostic potential. Proteomic studies also demonstrated that 3D-derived EVs exhibited increased total protein content, upregulated differentially expressed proteins, and enhanced surface marker expression.[35,45,52,60,61,64,72,75–80,93] However, four studies using dynamic bioreactors found a contrasting trend, with lower protein content per EV,[88–90,93] potentially due to the smaller EV size,[93] or flow-induced membrane shedding.[88] Flow-induced membrane shedding can occur when media flow in bioreactors exposes cells to low shear stress, promoting direct shedding of the cell membrane into the extracellular space and favoring the formation of microvesicles over exosomes.[88,99] Supporting this, one study confirmed a reduction in exosome-specific markers (*e.g.*, CD63-positive EVs) in bioreactor systems, indicating a dilution of the exosome population by microvesicles.[88] As microvesicles carry a distinct proteomic cargo compared to exosomes due to their differing biogenesis pathways, this shift likely contributes to the overall lower protein-to-EV ratio and altered EV composition.[16] These findings highlight the need for researchers to consider the effects of culture conditions like shear stress on EV biogenesis and composition.

Functional studies evaluating the therapeutic and diagnostic potential of EVs revealed enhanced functionality of 3D-derived EVs in most cases, such as increased invasion capacity of recipient cells, increased osteogenic potential, and

enhanced neuroregenerative and wound healing properties.[48,63,65,72,73,75–80,85,86,89,90,93] However, three studies reported reduced functionality or dysfunctionality of 3D-derived EVs.[46,52,61] Two studies used spheroid culture to aggregate MSCs,[46,52] while another employed a collagen hydrogel to culture human oral mucosal lamina propria-progenitor cells.[61] Reduced functionality in these cases may stem from limitations in the culture systems, such as impaired nutrient and oxygen diffusion in spheroid or static culture, leading to metabolic stress and altered exosome cargo. Moreover, the collagen hydrogel model may have restricted cell behavior due to its material properties, limiting the production of functional exosomes and reducing their therapeutic potential. These findings highlight the need to optimize spheroid size, scaffold materials, and culture conditions to maximize the therapeutic efficacy of EVs.

Overall, this review supports the transition from 2D to 3D culture systems for higher yield and more physiologically relevant EV research and production. 3D cultures offer higher yields, comparable or more physiologically relevant EV morphology, enriched genomic and proteomic cargo, and enhanced functionality. However, each type of 3D model presents distinct strengths and limitations that must be carefully considered based on research context.

Scaffold-free 3D models, such as hanging-drop or ULA plates, facilitate spheroid formation and cell-to-cell interactions, often resulting in enhanced EV yield and enriched miRNA or proteomic cargo.[42,45,48,52] These systems are simple and cost-effective, making them suitable for high-throughput applications. However, these models lack ECM components and dynamic mechanical cues, limiting their ability to fully recapitulate the native microenvironment. Additionally, variability in spheroid size, limited nutrient diffusion in larger aggregates, and challenges in long-term culture can impact EV quality and consistency.[46,52]

Scaffold-based 3D models using natural hydrogels (*e.g.*, collagen, Matrigel™, alginate, agarose) more closely mimic ECM architecture and biochemical composition, supporting enhanced EV secretion and bioactive cargo loading.[35,60,61,63,72,73] For example, collagen-based scaffolds have been shown to enrich EVs in tumor-associated mRNAs,[60] while Matrigel™ cultures produce EVs expressing invasion-associated miRNAs.[35] However, natural hydrogels suffer from batch-to-batch variability, limited tunability, and inconsistent mechanical properties, which may affect reproducibility.

Synthetic hydrogels, such as peptide-based matrices, offer improved reproducibility and tunability of porosity, stiffness, and degradability. Their ability to independently control mechanical and biochemical cues makes them ideal for studying how specific microenvironmental cues affect EV production and cargo loading. EVs produced in synthetic peptide hydrogels show increased secretion and enhanced similarity as reflected by their size and genomic cargo.[67] However, their limited bioactivity, higher cost, and potential instability over extended culture periods remain challenges for broader adoption.

Rigid and fibrous scaffolds, including 3D-printed scaffolds and natural fibrous scaffolds, offer structural integrity and mechanical properties suitable for modeling load-bearing tissues. These scaffolds allow for cell attachment, migration, and sustained culture, which can support long-term high-yield production of EVs with enhanced functionality.[75,76] Studies have shown that scaffold geometry and fiber orientation can influence EV yield and bioactivity, with aligned fibers or specific pore shapes enhancing osteogenic or angiogenic potential.[75] However, rigid scaffolds often lack the bioactivity of hydrogels and may limit cell–matrix remodeling, while their fabrication and material properties may restrict adaptability for soft tissue models. They are particularly useful for bone, cartilage, and musculoskeletal applications where mechanical strength and architecture are essential.

Dynamic 3D systems, such as perfusion and microcarrier-based bioreactors, represent some of the most advanced platforms for EV production. By enabling continuous nutrient and oxygen delivery along with mechanical stimulation, these systems can drastically enhance EV yield, with some studies reporting up to a 10 000-fold increase compared to 2D culture.[88] EVs derived from bioreactors have also consistently demonstrated improved therapeutic efficacy, including enhanced neuroregenerative and wound-healing effects *in vivo*.[79,80,84–86,88–90,93] However, these systems are more complex and expensive to operate, requiring careful optimization of parameters such as flow rate, scaffold architecture, and media exchange. Additionally, several studies reported reduced protein content per EV,[88–90,93] possibly due to shear stress or flow-induced membrane shedding, suggesting that bioreactors may be less suitable for applications requiring protein-rich vesicles unless these variables are tightly controlled.

In summary, no single model is universally superior; rather, the choice depends on the specific application. For high-throughput EV profiling or mechanistic studies, scaffold-free 3D systems offer a practical compromise between simplicity and relevance. For studies requiring tissue-specific EV cargo or therapeutic potency, scaffold-based and bioreactor models are more appropriate. Understanding the strengths and limitations of each system is essential for standardizing EV research and translating *in vitro* findings into clinically meaningful outcomes.

Data availability

No primary research results, software or code have been included and no new data were generated or analysed as part of this review.

Conflicts of interest

There are no conflicts to declare.

Acknowledgements

We acknowledge the support of the Cancer Research Society and the Canadian Institutes of Health Research (Funding Reference Number: 196962). K. C. thanks graduate scholarships from the University of Guelph.

References

1 Y. Couch, *et al.*, A brief history of nearly EV–erything – The rise and rise of extracellular vesicles, *J. Extracell. Vesicles*, 2021, **10**, DOI: 10.1002/jev2.12144.
2 B.-T. Pan and R. M. Johnstone, Fate of the transferrin receptor during maturation of sheep reticulocytes in vitro: Selective externalization of the receptor, *Cell*, 1983, **33**, 967–978.
3 C. Harding, J. Heuser and P. Stahl, Receptor-mediated endocytosis of transferrin and recycling of the transferrin receptor in rat reticulocytes, *J. Cell Biol.*, 1983, **97**, 329.
4 G. Raposo, *et al.*, B lymphocytes secrete antigen-presenting vesicles, *J. Exp. Med.*, 1996, **183**, 1161–1172.
5 J. Ratajczak, *et al.*, Embryonic stem cell-derived microvesicles reprogram hematopoietic progenitors: evidence for horizontal transfer of mRNA and protein delivery, *Leukemia*, 2006, **20**, 847–856.
6 J. Skog, *et al.*, Glioblastoma microvesicles transport RNA and proteins that promote tumour growth and provide diagnostic biomarkers, *Nat. Cell Biol.*, 2008, **10**, 1470–1476.
7 W.-H. Chang, R. A. Cerione and M. A. Antonyak, Extracellular Vesicles and Their Roles in Cancer Progression, *Methods Mol. Biol.*, 2021, **2174**, 143.
8 K. Al-Nedawi, *et al.*, Intercellular transfer of the oncogenic receptor EGFRvIII by microvesicles derived from tumour cells, *Nat. Cell Biol.*, 2008, **10**, 619–624.
9 M. A. Antonyak, *et al.*, Cancer cell-derived microvesicles induce transformation by transferring tissue transglutaminase and fibronectin to recipient cells, *Proc. Natl. Acad. Sci. U. S. A.*, 2011, **108**, 4852–4857.
10 C. A. Franzen, *et al.*, Urothelial cells undergo epithelial-to-mesenchymal transition after exposure to muscle invasive bladder cancer exosomes, *Oncogenesis*, 2015, **4**, e163.
11 H. Peinado, *et al.*, Melanoma exosomes educate bone marrow progenitor cells toward a pro-metastatic phenotype through MET, *Nat. Med.*, 2012, **18**, 883–891.
12 S. A. Ibrahim and Y. S. Khan, Histology, Extracellular Vesicles, in *StatPearls*, StatPearls Publishing, 2023.
13 M. Yáñez-Mó, *et al.*, Biological properties of extracellular vesicles and their physiological functions, *J. Extracell. Vesicles*, 2015, **4**, DOI: 10.3402/jev.v4.27066.
14 M. P. Zaborowski, L. Balaj, X. O. Breakefield and C. P. Lai, Extracellular Vesicles: Composition, Biological Relevance, and Methods of Study, *Bioscience*, 2015, **65**, 783–797.
15 V. Estévez-Souto, S. D. Silva-Álvarez and M. Collado, The role of extracellular vesicles in cellular senescence, *FEBS J.*, 2022, **290**, 1203–1211.
16 L. M. Doyle and M. Z. Wang, Overview of Extracellular Vesicles, Their Origin, Composition, Purpose, and Methods for Exosome Isolation and Analysis, *Cells*, 2019, **8**, 727.
17 D.-S. Sun and H.-H. Chang, Extracellular vesicles: Function, resilience, biomarker, bioengineering, and clinical implications, *Tzu Chi Med. J.*, 2024, **36**, 251.
18 T. Yamashita, *et al.*, Epidermal growth factor receptor localized to exosome membranes as a possible biomarker for lung cancer diagnosis, *Pharmazie*, 2013, **68**, 969–973.
19 Y. Zhang and H. Xu, Serum exosomal miR-378 upregulation is associated with poor prognosis in non–small-cell lung cancer patients, *J. Clin. Lab. Anal.*, 2020, **34**, e23237.
20 S. Langevin, *et al.*, Comprehensive microRNA-sequencing of exosomes derived from head and neck carcinoma cells in vitro reveals common secretion profiles and potential utility as salivary biomarkers, *Oncotarget*, 2017, **8**, 82459–82474.
21 A.-K. Rupp, *et al.*, Loss of EpCAM expression in breast cancer derived serum exosomes: Role of proteolytic cleavage, *Gynecol. Oncol.*, 2011, **122**, 437–446.
22 P. Moon, *et al.*, Fibronectin on circulating extracellular vesicles as a liquid biopsy to detect breast cancer, *Oncotarget*, 2016, **7**, 40189–40199.
23 X. Lai, *et al.*, A microRNA signature in circulating exosomes is superior to exosomal glypican-1 levels for diagnosing pancreatic cancer, *Cancer Lett.*, 2017, **393**, 86–93.
24 L.-Y. Lin, *et al.*, Tumor-originated exosomal lncUEGC1 as a circulating biomarker for early-stage gastric cancer, *Mol. Cancer*, 2018, **17**, 1–6.
25 Q. Li, *et al.*, Plasma long noncoding RNA protected by exosomes as a potential stable biomarker for gastric cancer, *Tumor Biol.*, 2015, **36**, 2007–2012.
26 R. Zhao, *et al.*, Exosomal long noncoding RNA HOTTIP as potential novel diagnostic and prognostic biomarker test for gastric cancer, *Mol. Cancer*, 2018, **17**, 1–5.
27 D. Li, S. Jia, S. Wang and L. Hu, Glycoproteomic Analysis of Urinary Extracellular Vesicles for Biomarkers of Hepatocellular Carcinoma, *Molecules*, 2023, **28**, 1293.
28 Y. H. Lin, T. M. Pan, M. H. Wu, A. K. Miri and D. Nieto, *Microfluidic Technology and Its Biological Applications*, 2019, pp. 62–80. DOI: 10.1016/B978-0-444-64046-8.00280-9.
29 S. Maji, *et al.*, Exosomal Annexin II Promotes Angiogenesis and Breast Cancer Metastasis, *Mol. Cancer Res.*, 2017, **15**, 93–105.
30 D. Albino, *et al.*, Circulating extracellular vesicles release oncogenic miR-424 in experimental models and patients with aggressive prostate cancer, *Commun. Biol.*, 2021, **4**, 1–13.
31 H. Keilová, The effect of streptomycin on tissue cultures, *Experientia*, 1948, **4**, 483–484.
32 T. Turner, Development of the Polio Vaccine: A Historical Perspective of Tuskegee University's Role in Mass Production and Distribution of HeLa Cells, *J. Health Care Poor Underserved*, 2012, **23**, 5.

33 D. Peehl and R. Ham, Clonal growth of human keratinocytes with small amounts of dialyzed serum, *In vitro*, 1980, **16**, 526–540.
34 J. Yu, *et al.*, Induced pluripotent stem cell lines derived from human somatic cells, *Science*, 2007, **318**, 1917–1920.
35 M. Schuster, *et al.*, Extracellular vesicles secreted by 3D tumor organoids are enriched for immune regulatory signaling biomolecules compared to conventional 2D glioblastoma cell systems, *Front. Immunol.*, 2024, **15**, 1388769.
36 D. Antoni, H. Burckel, E. Josset and G. Noel, Three-Dimensional Cell Culture: A Breakthrough in Vivo, *Int. J. Mol. Sci.*, 2015, **16**, 5517.
37 M. Casajuana Ester and R. M. Day, Production and Utility of Extracellular Vesicles with 3D Culture Methods, *Pharmaceutics*, 2023, **15**, 663.
38 P. R. Baraniak and T. C. McDevitt, Scaffold-free culture of mesenchymal stem cell spheroids in suspension preserves multilineage potential, *Cell Tissue Res.*, 2011, **347**, 701.
39 F. Shekari, *et al.*, Cell culture–derived extracellular vesicles: Considerations for reporting cell culturing parameters, *J. Extracell. Biol.*, 2023, **2**, DOI: **10.1002/jex2.115**.
40 C. Mas-Bargues and C. Borrás, Importance of stem cell culture conditions for their derived extracellular vesicles therapeutic effect, *Free Radicals Biol. Med.*, 2021, **168**, 16–24.
41 Low Attachment Cell Culture Plates, Dishes, and Flasks – CA, *ThermoFisher Scientific*, **https://www.thermofisher.com/ca/en/home/life-science/cell-culture/organoids-spheroids-3d-cell-culture/3d-cell-culture-plates-dishes-flasks.html**.
42 M. Kim, H.-W. Yun, D. Y. Park, B. H. Choi and B.-H. Min, Three-Dimensional Spheroid Culture Increases Exosome Secretion from Mesenchymal Stem Cells, *Tissue Eng. Regen. Med.*, 2018, **15**, 427–436.
43 O. Habanjar, M. Diab-Assaf, F. Caldefie-Chezet and L. Delort, 3D Cell Culture Systems: Tumor Application, Advantages, and Disadvantages, *Int. J. Mol. Sci.*, 2021, **22**, 12200.
44 M. C. Ester and R. M. Day, Production and Utility of Extracellular Vesicles with 3D Culture Methods, *Pharmaceutics*, 2023, **15**, 663.
45 J. Tu, X. Luo, H. Liu, J. Zhang and M. He, Cancer spheroids derived exosomes reveal more molecular features relevant to progressed cancer, *Biochem. Biophys. Rep.*, 2021, **26**, 101026.
46 G. D. Kusuma, *et al.*, Effect of 2D and 3D Culture Microenvironments on Mesenchymal Stem Cell-Derived Extracellular Vesicles Potencies, *Front. Cell Dev. Biol.*, 2022, **10**, 819726.
47 S. Zhu, *et al.*, Influence of experimental variables on spheroid attributes, *Sci. Rep.*, 2025, **15**, 1–13.
48 Y. Zhang, *et al.*, Exosomes derived from 3D-cultured MSCs improve therapeutic effects in periodontitis and experimental colitis and restore the Th17 cell/Treg balance in inflamed periodontium, *Int. J. Oral Sci.*, 2021, **13**, 1–15.
49 A. S. Nunes, A. S. Barros, E. C. Costa, A. F. Moreira and I. J. Correia, 3D tumor spheroids as in vitro models to mimic in vivo human solid tumors resistance to therapeutic drugs, *Biotechnol. Bioeng.*, 2019, **116**, 206–226.
50 X. Cui, Y. Hartanto and H. Zhang, Advances in multicellular spheroids formation, *J. R. Soc., Interface*, 2017, **14**, DOI: **10.1098/rsif.2016.0877**.
51 A. G. Mitrakas, *et al.*, Applications and Advances of Multicellular Tumor Spheroids: Challenges in Their Development and Analysis, *Int. J. Mol. Sci.*, 2023, **24**, 6949.
52 N. L. A. Khan, *et al.*, Effect of 3D and 2D cell culture systems on trophoblast extracellular vesicle physico-chemical characteristics and potency, *Front. Cell Dev. Biol.*, 2024, **12**, 1382552.
53 M. Rasouli, F. Safari, M. H. Kanani and H. Ahvati, *Principles of Hanging Drop Method (Spheroid Formation) in Cell Culture*, 2024, pp. 1–12. DOI: **10.1007/7651_2024_527**.
54 B. Pinto, A. C. Henriques, P. M. A. Silva and H. Bousbaa, Three-Dimensional Spheroids as In Vitro Preclinical Models for Cancer Research, *Pharmaceutics*, 2020, **12**, 1186.
55 S.-W. Huang, S.-C. Tzeng, J.-K. Chen, J.-S. Sun and F.-H. Lin, A Dynamic Hanging-Drop System for Mesenchymal Stem Cell Culture, *Int. J. Mol. Sci.*, 2020, **21**, 4298.
56 F. Ruedinger, A. Lavrentieva, C. Blume, I. Pepelanova and T. Scheper, Hydrogels for 3D mammalian cell culture: a starting guide for laboratory practice, *Appl. Microbiol. Biotechnol.*, 2015, **99**, 623–636.
57 S. R. Caliari and J. A. Burdick, A Practical Guide to Hydrogels for Cell Culture, *Nat. Methods*, 2016, **13**, 405.
58 I. M. El-Sherbiny and M. H. Yacoub, Hydrogel scaffolds for tissue engineering: Progress and challenges, *Glob. Cardiol. Sci. Pract.*, 2013, **2013**, 38.
59 J. Insua-Rodriguez and T. Oskarsson, The extracellular matrix in breast cancer, *Adv. Drug Delivery Rev.*, 2016, **97**, 41–55.
60 A. Villasante, *et al.*, Recapitulating the Size and Cargo of Tumor Exosomes in a Tissue-Engineered Model, *Theranostics*, 2016, **6**, 1119–1130.
61 Y. Yang, R. Knight, P. Stephens and Y. Zhang, Three–dimensional culture of oral progenitor cells: Effects on small extracellular vesicles production and proliferative function, *J. Oral Pathol. Med.*, 2019, **49**, 342–349.
62 F. Jiang, *et al.*, Extraction, Modification and Biomedical Application of Agarose Hydrogels: A Review, *Mar. Drugs*, 2023, **21**, 299.
63 S. Rocha, *et al.*, 3D Cellular Architecture Affects MicroRNA and Protein Cargo of Extracellular Vesicles, *Adv. Sci.*, 2018, **6**, 1800948.
64 M. Peshkova, *et al.*, Four sides to the story: A proteomic comparison of liquid–phase and matrix–bound extracellular vesicles in 2D and 3D cell cultures, *Proteomics*, 2024, **24**, e2300375.
65 E. D. Quiñones, *et al.*, Extracellular vesicles from human adipose-derived stem cell spheroids: Characterization and therapeutic implications in diabetic wound healing, *Mater. Today Bio*, 2024, **29**, 101333.
66 P. Worthington, D. J. Pochan and S. A. Langhans, Peptide Hydrogels – Versatile Matrices for 3D Cell Culture in Cancer Medicine, *Front. Oncol.*, 2015, **5**, 92.

67 S. Thippabhotla, C. Zhong and M. He, 3D cell culture stimulates the secretion of in vivo like extracellular vesicles, *Sci. Rep.*, 2019, **9**, 1–14.
68 R. Swarm, Transplantation Of A Murine Chondrosarcoma In Mice Of Different Inbred Strains, *J. Natl. Cancer Inst.*, 1963, **31**, 953–975.
69 R. W. Orkin, *et al.*, A murine tumor producing a matrix of basement membrane, *J. Exp. Med.*, 1977, **145**, 204–220.
70 K. K. Hynda and G. Martin, Matrigel: Basement membrane matrix with biological activity, *Semin. Cancer Biol.*, 2005, **15**, 378–386.
71 A. Passaniti, H. K. Kleinman and G. R. Martin, Matrigel: history/background, uses, and future applications, *J. Cell Commun. Signal.*, 2021, **16**, 621.
72 J. Chen, *et al.*, A scalable coaxial bioprinting technology for mesenchymal stem cell microfiber fabrication and high extracellular vesicle yield, *Biofabrication*, 2021, **14**, 015012.
73 W. Zhang, *et al.*, Three-dimensional cell culture-derived extracellular vesicles loaded alginate/hyaluronic acid composite scaffold as an optimal therapy for cartilage defect regeneration, *Biomed. Mater.*, 2025, **20**, 025021.
74 M. DiCerbo, M. M. Benmassaoud and S. L. Vega, Porous Scaffold-Hydrogel Composites Spatially Regulate 3D Cellular Mechanosensing, *Front. Med. Technol.*, 2022, **4**, 884314.
75 K. Man, *et al.*, Development of a Bone-Mimetic 3D Printed Ti6Al4 V Scaffold to Enhance Osteoblast-Derived Extracellular Vesicles' Therapeutic Efficacy for Bone Regeneration, *Front. Bioeng. Biotechnol.*, 2021, **9**, 757220.
76 W. Gao, *et al.*, Exosomes from 3D culture of marrow stem cells enhances endothelial cell proliferation, migration, and angiogenesis via activation of the HMGB1/AKT pathway, *Stem Cell Res.*, 2021, **50**, 102122.
77 Y. Zhang, *et al.*, Systemic administration of cell-free exosomes generated by human bone marrow derived mesenchymal stem cells cultured under 2D and 3D conditions improves functional recovery in rats after traumatic brain injury, *Neurochem. Int.*, 2017, **111**, 69–81.
78 P. Hu, *et al.*, Exosomes of adult human fibroblasts cultured on 3D silk fibroin nonwovens intensely stimulate neoangiogenesis, *Burns Trauma*, 2021, **9**, tkab003.
79 R. A. Haraszti, *et al.*, Exosomes Produced from 3D Cultures of MSCs by Tangential Flow Filtration Show Higher Yield and Improved Activity, *Mol. Ther.*, 2018, **26**, 2838–2847.
80 E. Jalilian, *et al.*, Bone marrow mesenchymal stromal cells in a 3D system produce higher concentration of extracellular vesicles (EVs) with increased complexity and enhanced neuronal growth properties, *Stem Cell Res. Ther.*, 2022, **13**, 425.
81 M. Stephenson and W. Grayson, Recent advances in bioreactors for cell-based therapies, *F1000Research*, 2018, **7**, F1000 Faculty Rev–517.
82 F. Palladino, *et al.*, Bioreactors: Applications and Innovations for a Sustainable and Healthy Future—A Critical Review, *Appl. Sci.*, 2024, **14**, 9346.
83 Thermo Fisher Scientific, Perfusion: Planning a Run, White paper, **https://assets.thermofisher.com/TFS-Assets/BPD/Reference-Materials/perfusion-planning-run-white-paper.pdf**, accessed February 2, 2025.
84 L. Sun, *et al.*, A 3D culture system improves the yield of MSCs-derived extracellular vesicles and enhances their therapeutic efficacy for heart repair, *Biomed. Pharmacother.*, 2023, **161**, 114557.
85 J. Cao, *et al.*, Three-dimensional culture of MSCs produces exosomes with improved yield and enhanced therapeutic efficacy for cisplatin-induced acute kidney injury, *Stem Cell Res. Ther.*, 2020, **11**, 1–13.
86 L. Yan and X. Wu, Exosomes produced from 3D cultures of umbilical cord mesenchymal stem cells in a hollow-fiber bioreactor show improved osteochondral regeneration activity, *Cell Biol. Toxicol.*, 2020, **36**, 165–178.
87 D. C. Watson, *et al.*, Efficient production and enhanced tumor delivery of engineered extracellular vesicles, *Biomaterials*, 2016, **105**, 195–205.
88 D. B. Patel, C. R. Luthers, M. J. Lerman, J. P. Fisher and S. M. Jay, Enhanced extracellular vesicle production and ethanol-mediated vascularization bioactivity via a 3D-printed scaffold-perfusion bioreactor system, *Acta Biomater.*, 2019, **95**, 236–244.
89 S. M. Kronstadt, *et al.*, Mesenchymal stem cell culture within perfusion bioreactors incorporating 3D-printed scaffolds enables improved extracellular vesicle yield with preserved bioactivity, *Adv. Healthcare Mater.*, 2023, **12**, e2300584.
90 E. H. Powsner, K. Nikolov and S. M. Jay, Integrating cell confinement in a perfusion bioreactor improves iMSC extracellular vesicle production and potency, *Cytotherapy*, 2025, **27**, S87–S88.
91 Exploring Different Types of Bioreactors for Bioprocessing: A Comprehensive Overview of Wave Bioreactors and Alternative Systems for Cell Culture, Fermentation, and Biopharmaceutical Production, *Food4Innovations (EN) - Wouter de Heij M.Sc.*, **https://wouterdeheij.com/2023/06/13/exploring-different-types-of-bioreactors-for-bioprocessing-a-comprehensive-overview-of-wave-bioreactors-and-alternative-systems-for-cell-culture-fermentation-and-biopharmaceutical-production/**, 2023.
92 I. Slivac, V. G. Srček, K. RadoŠević, I. Kmetič and Z. Kniewald, Aujeszky's disease virus production in disposable bioreactor, *J. Biosci.*, 2006, **31**, 363–368.
93 X. Yuan, *et al.*, Engineering extracellular vesicles by three–dimensional dynamic culture of human mesenchymal stem cells, *J. Extracell. Vesicles*, 2022, **11**, e12235.
94 B. Koh, *et al.*, Three dimensional microcarrier system in mesenchymal stem cell culture: a systematic review, *Cell Biosci.*, 2020, **10**, 1–16.
95 B. Li, *et al.*, Past, present, and future of microcarrier-based tissue engineering, *J. Orthop. Transl.*, 2015, **3**, 51.
96 P. M. Neto, *et al.*, Characterization of the Aeration and Hydrodynamics in Vertical-Wheel™ Bioreactors, *Bioengineering*, 2022, **9**, 386.
97 B. S. Borys, *et al.*, Overcoming bioprocess bottlenecks in the large-scale expansion of high-quality hiPSC aggregates

in vertical-wheel stirred suspension bioreactors, *Stem Cell Res. Ther.*, 2021, **12**, 1–19.

98 L. E. Freed and F. Guilak, *Principles of Tissue Engineering*, Academic Press, 2007.

99 S. EL Andaloussi, I. Mäger, X. O. Breakefield and M. J. A. Wood, Extracellular vesicles: biology and emerging therapeutic opportunities, *Nat. Rev. Drug Discovery*, 2013, **12**, 347–357.